THE ROLE OF MOISTURE SCHEME IN REGIONAL CLIMATE MODELLING OF PRECIPITATION OVER THE HORN OF AFRICA

By

ABEBE KEBEDE H/GEBRIEL

SUBMITTED IN PARTIAL FULFILLMENT OF THE
REQUIREMENTS FOR THE DEGREE OF
MASTER OF SCIENCE IN PHYSICS
AT
ADDIS ABABA UNIVERSITY
ADDIS ABABA, ETHIOPIA
JUNE 2011

ADDIS ABABA UNIVERSITY
DEPARTMENT OF
PHYSICS

Supervisor: _____
DR. GIZAW MENGISTU

Examiners: _____
DR. ELIAS LEWI

_____
DR. LEMI DEMEYU

ADDIS ABABA UNIVERSITY

Date: **JUNE 2011**

Author: **ABEBE KEBEDE H/GEBRIEL**

Title: **THE ROLE OF MOISTURE SCHEME IN REGIONAL CLIMATE MODELLING OF PRECIPITATION OVER THE HORN OF AFRICA**

Department: **Physics**

Degree: **M.Sc.** Convocation: **JUNE** Year: **2011**

Permission is herewith granted to Addis Ababa University to circulate and to have copied for non-commercial purposes, at its discretion, the above title upon the request of individuals or institutions.

Signature of Author

Table of Contents

List of Figures

List of Tables

ABSTRACT

This study aims to improve the capability of the latest Regional Climate Model version 4 (RegCM4) to simulate the precipitation over the Horn of Africa. Although there are several aspects in which the model can be improved, the focus of this study is to tackle the problem of its moisture scheme. RegCM4 moisture scheme has fourteen moisture scheme parameters, which can be tuned within the allowed physical limits. Each of the 14 moisture parameters have been varied around the current default setting and over 80 model runs have been performed, for a domain defined by 60km resolution, 18 vertical levels covering nearly the whole Africa geographycally and major circulation patterns that derive climate over the region. We have found physical sound set of parameters to be used in the fourteen moisture scheme parameters that have siginificantly reduced bias in RegCM4 pricipitation; improved correlation of RegCM4 precipitation with respect GPCP and CMAP; and captured seasonal and interannual variations over most of the 12 delineated homogeneous regions of Horn of Africa.

ACKNOWLEDGEMENTS

I would like to express my sincere thanks to my advisor and instructor Dr. Gizaw Mengistu for his guidance, assistance, supervision and contribution of valuable suggestions. His scientific excitement, integral view on research and overly enthusiasm, has made a deep impression on me.

I would like to thank to all my fellow students for providing encouragement and support in the Atmospheric Optics and Computational Lab. 2010–2011.

Chapter 1

INTRODUCTION

The Horn of Africa (HOA) has distinct climate characteristics compared to the rest of the continent by Vojtesak et al. (1990). The HOA is replete with complex terrain comprising of some of the known tropical high mountains and the Great Rift Valley System (GRVS). As a whole the complex HOA terrain presents an enabling environment where local and large scale climate systems frequently interact to create highly variable climate in both space and time.

At the same time, inter-annual variability of the HOA climate is linked to perturbations in the global SSTs, especially over the equatorial Pacific and Indian Ocean basins, and to some extent, the Atlantic Ocean. These three global oceans, all at the same time or each at different times, intriguingly influence the interannual variability of the HOA climate. Interactions and feedbacks among these multiple climate drivers over the region present challenges in quantitative understanding of regional climate variability and changes based on typical empirical techniques. Therefore, there is a need to employ physically-based, regional climate models (RCM) that can offer scope and capability to unveil cause-effect relationships between regional climate variability and individual or combination of processes. However, representation of the multiple sources of forcing to the HOA climate also poses a great challenge to RCM as well.

For hydrological cycle the presence of clouds and resulting precipitation is the primary control on the cycles. The ERA-Intrim reanalysis corrects some of the errors of the

ERA-40 reanalysis particularly in the hydrological cycles variables over the tropics. It is also important to accurately represent cloud processes in many modelling application. Clouds are often poorly represented in both regional and global climate models (RCMs and GCMs) respectively pal. et al (2000).

This study aims to improve nonconvective moist physics and cloud scheme used in RegCM4 that accounts for the subgrid variability of clouds: rain drop accretion rate, rain drop evaporation rate temperature threshold, autoconversion rate, gultape equation, relative humidity, maximum fractional cloud, temperature, cloud liquid water content for convective and maximum cloud fractional cover for convective precipitation. This parameters are catagorized under nonconvective precipitation parameterization called subgrid explicit moisture (SUBEX) in RegCM4. We have varied the fourteen parameters under SUBEX with the allowed physical limits of the parameter in an effort to improve precipitation simulation of Horn of Africa region. The atmosphere variability over this region comparable to the size of the model grid cell often results in saturated areas where cloud exist subsaturated, areas where cloud does exist.

Chapter 2

LONG TERM MEAN CLIMATE OF THE HORN OF AFRICA

The geography, general climatic controls, and long term mean (LTM) climate of the HOA are well described in a comprehensive set of Air Force Combat Climatology Center (AFCCC) publications. Of these, Vojtesak et al. (1990) is the most complete as it compiles most important aspects of the LTM regional climate in one source.

The information provided by Vojtesak et al. (1990) is currently being updated (from a long term mean perspective) one country at a time by AFCCC in a series of publications by Giese (e.g., Giese 2004, 2005), but it will be some time before a full update is complete. Additionally, shorter AFCCC narratives capture the LTM climate down to the city, town, and even village level, as well.

2.1 Geography of the Horn of Africa

The focus of this research is on the portions of the horn of Africa (HOA) contained within the political boundaries of Eritrea, Ethiopia, Djibouti, Somalia, and Yemen plus neighboring countries of east Africa referred to as the Greater HOA. The ensuing discussion is heavily paraphrased from Vojtesak et al. (1990), which contains a succinct description of the geography and LTM climate of the HOA. Geographically, the western half of the HOA is dominated by the Great Rift mountain system, which runs nearly the entire length of east Africa, extending into the Arabian Peninsula in the extreme north. These mountains

average 2133.6–2438.4 meters in height, with some peaks topping 3048–3657.6 meters. The mountains have a marked influence on climate and weather in the HOA, presenting a major natural barrier between modified maritime and continental tropical air masses to the west, and Indian Ocean (IO) maritime tropical air to the east. The only locations below 850 hPa where air masses from the east and west can converge and interact are the Red Sea - Gulf of Aden corridor and the Turkana Channel in northern Kenya.

The eastern half of the HOA can be largely characterized as an alluvial plain, lying at elevations of about 914.6 meters or less. The terrain slopes upward from east to west, transitioning from lowlands at the shorelines, then to rolling hills and plateau, until meeting the Great Rift mountain chain.

Figure 2.1: Horn of Africa

The complexities of terrain in the HOA make an understanding of local effects key to weather and climate forecasting. Major local factors include elevation, latitude, terrain, and orientation of topographic features to the prevailing large scale flow.

With this in mind, Vojtesak et al. (1990) partitioned the HOA into four regions of homogeneous topography, weather, and climate, so called zones of climatic commonality. This

approach is very useful in simplifying the discussion of the local features and climate from both scientific and operational perspectives.

The Aden Coastal Fringe is the narrow strip of territory that lies along the Gulf of Aden and Red Sea coastlines. It includes coastal portions of Somalia, Djibouti and Yemen. The Indian Ocean (IO) Plains are, essentially, the coastal regions of the HOA, excluding the Aden Coastal Fringe. The Ethiopian Highlands region encompasses most of Ethiopia, as well as small portions of Djibouti, Somalia, and Sudan. The terrain here is mountainous with an average elevation of 1524 meters. The Yemen Highlands lie along the south-eastern edge of the Red Sea on the Arabian Peninsula, the only sub-region far enough north to experience more than infrequent passages of midlatitude weather systems. This sub-region is mountainous, with average elevations of 1828.8 meters and is bounded by the large Saharan and Rub al Khali deserts.

2.2 General Circulation and the Seasonal Cycle

Large-scale tropospheric circulation features influencing the HOA are largely controlled by (or can be associated with) the Asian monsoon, a seasonal reversal of winds caused by hemispheric-scale, continent-ocean temperature gradients (Ramage et al. 1971; Slingo et al. 2003).

The Asian monsoon affects wind flow at all levels, including lower and upper level jet streams such as the Somali Jet (SJ) and Tropical Easterly Jet (TEJ), and semi permanent high and low pressure systems.

These features are manifested in the local weather and climate in a variety of ways, depending upon such factors as orientation of terrain to broad-scale flow, and mesoscale effects like land-sea breezes and mountain valley winds. During winter (December –March), intense cold over the Asian continent results in subsidence and high surface pressures that peak in January. Low-level winds flow away from the high pressure region, resulting in a

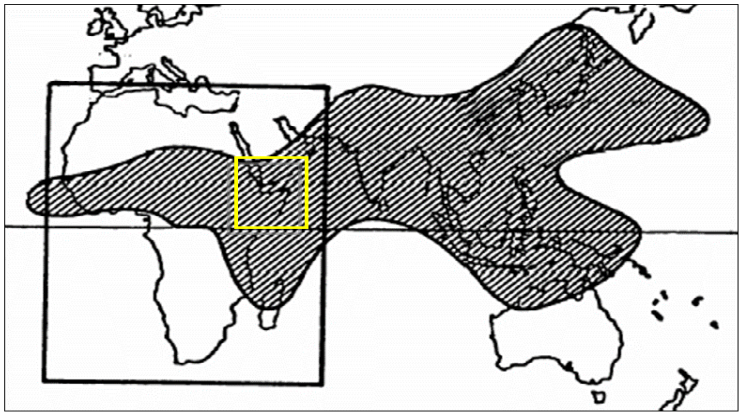

Figure 2.2: Asian monsoon [From Lajoie (2006)]

dry northeasterly surface flow out of Asia, into the HOA, and across the equator into the southern hemisphere.

During summer (June-September), the process and circulation are approximately opposite: intense heating over Asia results in convection and low surface pressures, reaching a peak in July . Cross-equatorial flow out of the Mascarene High from the southern hemisphere is deflected to the right by Coriolis effects and directed toward Asia. The overall pattern is a winter-summer reversal of the low-level winds from northeasterly to southwesterly.

Spring (April-May) and autumn (October-November) are transition seasons between the onset and cessation of the summer and winter monsoons. In the HOA, the seasons are referred to by a variety of names (e.g., Der, Gu, Masika, etc.) depending upon local vernacular. These terms describe the long rains that occur in the spring and the short rains in the autumn.

Much more precipitation falls during the long rains, while the short rains are more variable from year to year (Ogallo 1999). The HOA seasonal rains are triggered locally by the passage of the Inter-tropical Convergence Zone (ITCZ), a transient area of disturbed weather that marks the boundary between southerly flow and northerly flow. The ITCZ migrates north to south (south to north) during the boreal winter (summer), lagging the

overhead position of the sun by about 5^0 of latitude. However, the progression of the ITCZ can vary greatly locally due to complex terrain or other factors, such as the influence of climate variations on the Asian monsoon (Ogallo 1999).

The rainfall response to the ITCZ is highly variable. In extremely arid regions, such as Djibouti, for example, the passage of the ITCZ is ordinarily distinguished by little more than a shift in the predominant low-level flow, while more equatorial regions can experience significant shifts in rainfall.

Chapter 3

CLIMATE VARIATIONS AND THE HORN OF AFRICA

Long term mean climate is not comprehensive because they fail to take into account significant climate variations such as El Niño/La Niña. A climate variation is a persistent deviation from the LTM value of a climate system variable (e.g., temperature, winds, pressure, precipitation, etc.) (Murphree 2005). A persistent deviation is generally considered to be one that lasts for a week or longer. This makes them important in extended range forecasting (e.g., medium range, long range, and seasonal forecasts), which is especially valuable to military planners. Climate variations can be categorized according to their period (the time the variation lasts). The first is intraseasonal variations, which lasts from a week to approximately two months. A major example of an intraseasonal oscillation is the Madden-Julian Oscillation (MJO). The second major category is interannual variations, lasting from one to five years. Examples include El Niño/La Niña, Indian Ocean Zonal Mode (IOZM), and North Atlantic Oscillation (NAO). The third category is decadal variations. A decadal climate variation lasts from five to 30 years, and examples include the Pacific Decadal Oscillation (PDO).

There will be intraseasonal and interannual climate variations, with special consideration given to El Niño and La Niña and the IOZM, the interactions of the two, and their joint and individual influences on precipitation variability in the HOA.

3.1 El Niño and La Niña

During an El Niño or La Niña event, a complex and interconnected chain of climate variations occur across the tropical Pacific as the atmosphere-ocean system redistributes thermal energy. El Niño and La Niña events have a period of about two to seven years. They tend to begin in May-June and last approximately a year, reaching their maximum intensity in the tropics during November-February (Murphree 2005). These events have ramifications for the global circulation ranking only behind the change of seasons in importance and magnitude (Philander 1990).

Anomalous patterns and processes in the tropical Pacific are associated with El Niño/La Niña . El Niño and La Niña events and their impacts can be thought of as a sequence of anomalous events (Murphree 2005). For El Niño events, a basic chain of events is as follows:

1. Pacific subtropical highs become anomalously low and/or lows in the southeast Asian - western tropical Pacific become anomalously high;

2. The Pacific trades, which are the surface part of the Hadley-Walker Circulation (HWC), become correspondingly weak (strong);

3. Sea surface temperature (SST) becomes anomalously cool (warm) in the western (eastern) tropical Pacific;

4. Tropical convection become anomalously weak (strong) in the western (eastern) tropical Pacific; and

5. Energy, moisture, and momentum transports into and out of the tropical Pacific becomes anomalous in many ways.

The anomalous processes associated with La Niña are approximately opposite to those of El Niño, and have been described as extreme versions of the normal (Philander 1990). The differences in atmospheric and oceanic processes between normal El Niño and La Niña periods are clearly seen in the global HWC, SST anomalies and atmospheric and

oceanic structure in the tropical Pacific.

3.1.1 El Niño and La Niña Linkage to the HOA

Researchers have explored links between Linking El Niño and La Niña and precipitation in the HOA using a wide variety of data and methods. Their findings are diverse due to the extremely complex local effects and rainfall patterns in the HOA, but general consensus has been reached on several major points. First, El Niño and La Niña can be statistically linked, at least weakly, to precipitation variability in the HOA. Second, the season with the most robust precipitation response to El Niño and La Niña seems to be the boreal autumn.

El Niño and La Niña links to other seasons are weak or inconsistent, and all but ruled out in the literature. This may be because anomalies associated with El Niño and La Niña events peak in the Pacific during the boreal autumn-winter (Philander 1990).

HOA anomalies associated with El Niño and La Niña appear to be approximately opposite, with, for example, anomalously high (low) rainfall observed during El Niño(La Niña) years. Finally, the HOA response to La Niña seems to be more inconsistent and nonlinear. Two studies by Ropelewski and Halpert (1987, 1989) employed harmonic analysis and other statistical techniques to examine relationships between surface observations (precipitation and temperature) and the Southern Oscillation Index (SOI) at a global scale. The SOI is a measure of the seasonal fluctuations in the sea level pressure difference between Tahiti and Darwin. Negative (positive) values of the SOI correspond to El Niño (La Niña) periods. They identified consistent seasonal, regional precipitation and temperature anomalies for 19 (15) regions of the globe during El Niño(La Niña) events. This study documented a tendency for increased (decreased) northern hemisphere winter precipitation (temperatures) over parts of equatorial east Africa during El Niño events. Using the same techniques in a later study, Ropelewski and Halpert (1989) found roughly opposite responses in the same regions of the globe during La Niña events, though the

statistical relationships were not as strong. A later study by Ropelewski and Halpert (1995) noted, however, that the earlier analyses may have been too simple to quantify the complexities of rainfall for equatorial east Africa.

Farmer et al. (1988) used linear regression to study correlations between a long time series (1901-1984) of precipitation from four coastal Kenyan meteorological stations and the SOI. They found increased (decreased) rainfall during the autumn short rains for El Niño(La Niña) years, and a direct correlation between precipitation and the SOI. They also conjectured that improved forecasting skill seemed plausible using June August SOI to predict September-December rainfall.

A series of studies led by Ogallo (Ogallo 1988; Ogallo et al. 1988; Ogallo 1989) employed more sophisticated statistical methods (e.g., principle components analysis, factor analysis, etc.) and greatly expanded precipitation datasets (approximately 90 reporting stations in east Africa plus the Coupled Ocean-Atmosphere Data Set (COADS)) to examine links between El Niño and La Niña and sub-regional precipitation variability across portions of east Africa (Kenya, Uganda, Tanzania).

Precipitation records in each study were areally averaged and segregated into multiple homogeneous sub-regions with respect to rainfall in order to minimize undesirable variability due to local effects. Ogallo (1988) used SOI as a predictor for precipitation variability in each sub-region, while Ogallo et al. (1988) used global SST anomalies (SSTA). Each study reinforced and expanded the Farmer et al. (1988) findings that positive (negative) precipitation anomalies in equatorial east Africa during boreal autumns are associated with El Niño (La Niña), with the strongest associations in coastal regions.

In Ogallo (1988) it was noted for the first time, in passing, that positive SST anomalies in the IO and Arabian Sea were positively correlated with enhanced boreal autumn precipitation. These anomalies were apparently associated with a weakened northeast (NE) monsoon and attendant strengthening of cross-equatorial southeasterly (SE) flow during the boreal autumn, though mechanisms for these associations were not proposed.

Ogallo (1988) also found the La Niña precipitation response to be somewhat weaker and more inconsistent from event to event.

Beltrando (1990), and Hutchison (1992) employed roughly similar methods to those used by Farmer et al. (1988) to investigate the possibility of using the SOI as a predictive tool for rainfall in Somalia during April-July and September December. Correlations between prior season SOI values and summer precipitation proved insignificant, and links between the SOI and northwest Somalia were non existent. This is consistent with the findings of the earlier studies discussed.

However, correlations were found between June-August SOI values and September-December rainfall for southern and central Somalia. Each study found rainfall amounts to be high (low) for low (high) SOI values, corresponding to Pacific El Niño (La Niña) events.

3.1.2 El Niño and La Niña Linkage to the HOA through the IO

Beltrando and Camberlin (1993) computed linear correlations between IO surface pressure, IO SSTs, and areally averaged Somali precipitation records to assess the influence of IO conditions on the HOA.

They found that the autumn rains were negatively (positively) correlated with surface pressure, and positively (negatively) correlated with SST, in the western (eastern) IO.

Through correlations of Somali precipitation with the SOI, they substantiated earlier findings that autumn rainfall is generally above (below) average during El Niño (La Niña) events.

Hastenrath et al. (1993) explored the IO SST-HOA precipitation link during El Niño and La Niña conditions. From a comprehensive set of observational datasets assembled from multiple sources, Hastenrath et al. (1993) constructed indices for key atmospheric and oceanic variables (e.g., SST, vector winds, cloudiness, currents, etc.), statistically evaluated them, then outlined a hypothesized mechanism and sequence of events for rainfall

variability during the Apr-May and Oct-Nov transition seasons in east Africa, including the HOA.

They found that during an average year, a zonal Walker circulation exists across the equatorial IO with easterlies aloft and westerlies at low-levels with subsidence over the extreme western IO and HOA. The low level westerlies induce eastward upper ocean currents in the equatorial IO that help create relatively cool (warm) SSTs in the western (eastern) IO. Southwesterly winds along the HOA coast induce coastal upwelling and relatively cool SSTs that enhance the zonal pressure gradient that forces the low level westerlies.

In the spring and autumn transition seasons during El Niño(La Niña) years, the eastward pressure gradient force that drives the low level westerlies becomes anomalously strong (weak), presumably due to corresponding anomalies in convection over the maritime continent. This tends to intensify (weaken) both the climatological westerlies and eastward ocean currents, resulting in increased (decreased) subsidence over east Africa, as well as decreased (increased) moisture convergence, cloudiness, and precipitation across the region. Interestingly, they found that these effects are especially amplified during a La Niña year.

They attribute this to a strengthened summer monsoon during La Niña years that tends to reinforce an anomalously cold western IO, which in turn reinforces the mechanism. They also found that these effects are much stronger during the boreal autumn than it is in the boreal spring, similar to past studies.

Hastenrath et al. (1993) provided the first detailed and explicit mechanisms for HOA precipitation variability. Hastenrath et al. (2004) attempted to develop a predictive scheme based on precursor processes in the months leading up to the autumn short rains. The study reaffirmed that these anomalous processes occur during both transition seasons, but that the effect is much stronger during the boreal autumn. They also found that 70 percent of the interannual autumn rainfall variability could be accounted for by the concurrent intensity of the equatorial zonal Walker circulation in the IO. However, they

could not identify any clear precursors, and had no success in developing a predictive scheme.

A series of studies by Nicholson and co-authors (Nicholson 1997; Nicholson and Kim 1997; Nicholson and Selato 2000) used a modified version of the harmonic analysis techniques employed by Ropelewski and Halpert to examine the links between El Niño and La Niña, SSTs, and African precipitation variability. In an analysis that included all El Niño and La Niña events since 1901, they established strong links between El Niño and rainfall over many regions of the African continent.

For east Africa and the western IO, they found enhanced (suppressed) rainfall during El Niño and La Niña years, especially during the boreal autumn. The El Niño and La Niña rainfall anomalies were approximately opposite, but the El Niño anomalies were weaker. Perhaps the most significant finding in this series of studies was by Nicholson and Kim (1997). They observed that El Niño and La Niña influences were confined to those episodes which induced SST anomalies in the IO. Together with the Hastenrath papers, these are the chief early studies to conclude that El Niño and La Niña influences eastern African precipitation by forcing anomalies in atmospheric circulation that, in turn, impact IO SSTs.

3.2 The Indian Ocean Zonal Mode (IOZM)

Once researchers established that IO SSTs are a primary factor in forcing precipitation variability in the HOA, particularly in coastal and equatorial regions, the scientific community began conducting more in-depth examinations of processes that cause IO SST variability. This research led to identification of the Indian Ocean Zonal Mode (IOZM). The IOZM is an interannual, coupled atmosphere-ocean mode that creates anomalous SST patterns in the tropical IO. The IOZM are derived from Saji et al. (1999) and Webster et al. (1999), the first papers to explicitly describe the climate variation and its

association with anomalous precipitation in the HOA.

Under normal conditions, IO SSTs are slightly warmer (cooler) in the east (west). Through air-sea interactions, this SST gradient induces a west to east pressure gradient force and an equatorial zonal Walker circulation with westerlies (easterlies) in the lower (upper) troposphere. During a positive IOZM event, SSTs become anomalously warm (cold) temperatures in the western (eastern) IO, and vice versa for a negative IOZM event. The mechanisms and evolution of the IOZM have been identified by analyzing composites of multiple (Saji et al. 1999) and individual strong events (Webster 1999). Saji et al. (1999) examined composites of the extreme positive IOZM events of 1961, 1967, 1972, 1982, 1994, and 1997, and described the phenomena as follows.

Initially, cool SST anomalies appear in the equatorial eastern IO in May or June, accompanied by concurrent, moderate southeasterly wind anomalies in the southeastern tropical IO. Through the summer months, cold anomalies in the eastern IO intensify, and extend westward along the equator. The western tropical IO warms, especially off the coast of east Africa from northern Mozambique to northern Somalia, thereby setting up an anomalous SST dipole across the IO. This dipole gives rise to the term Indian Ocean Dipole (IOD) that is also used to refer to the conditions described by the term IOZM.

As this anomalous SST dipole develops, the equatorial surface westerlies across the IO weaken. In conjunction with the SST and wind anomalies, anomalous strong convection and precipitation results over much of the northern half of eastern Africa and the western IO. At the same time, negative precipitation anomalies develop over the maritime continent.

IOZM events are characterized by SSTA dipoles that are referred to as positive or negative, leading to the terms positive IOZM (or IOD) event and negative IOZM (or IOD) event. Positive or negative IOZM events are often preceded in the year prior by an event of opposite sign. The intensity of the dipole is measured by the dipole mode index (DMI),

which is defined by Saji et al. (1999) as the difference in SST anomaly between the western tropical (50^0E to 80^0E, 10^0S to 10^0N) and eastern tropical (90^0E to 110^0E, 10^0S to equator) Indian Ocean.

The evolution of the IOZM appears to be phase locked to the seasonal cycle, intensifying during late spring through autumn, with a dramatic peak of anomalous features in October, followed by a rapid demise with the approach of the boreal winter. IOZM events usually end in November, but termination can be variable from year to year. Some events terminate as early as August, while an extreme event (e.g., 1961) can last well into January. Both Webster et al. (1999) and Saji et al. (1999) speculate that the onset and termination of IOZM events are forced by and strongly dependent upon the cycle of the Asian summer monsoon. If so, then deviations in the intensity, timing, or location of monsoon circulation components would impact the IOZM.

3.2.1 Interactions of El Niño and La Niña, IOZM, and HOA Precipitation

Most IO climate researchers now agree that IO SSTs are a major factor in forcing precipitation variability in the HOA, particularly in coastal regions during the autumn short rains, and that IO SST variability can be forced by internal or external mechanisms. However, they differ on the relative roles of and interactions between El Niño and La Niña, the IOZM, and IO SST anomalies.

The IOZM may be an independent entity with self maintained dynamics internal to the IO (e.g., Saji et al. 1999, Webster et al. 1999, Yamagata et al. 2002). It could be completely dependent upon forcing from, or a simple extension of, Pacific SST anomalies the Indonesian throughflow region during strong El Niño and La Niña events (Chambers et al. 1999). Recent research indicates that the likely answer may lie somewhere in the middle of these two opposing views (Black et al. 2003).

Saji et al. (1999) contended that the IOZM is relatively independent of El Niño and La Niña, driven by dynamics internal to the IO, and they present several findings to support this contention. In a time series of Dipole Mode Index(DMI) plotted against the NINO3 SST index and IO SSTs, they showed that IOZM and El Niño and La Niña events have distinct patterns of evolution, with onset, termination, and peaks at different times. SST patterns differed as well between IOZM and El Niño events. During El Niño a general, basin-wide warming across the IO was found, while IOZM events were characterized by a striking sea surface temperature anomaly (SSTA) dipole. They also pointed out that the very strong 1987 El Niño event was not an IOZM year, and a strong IOZM event during 1994 was not accompanied by an El Niño event. They argued that co-occurrences of strong El Niño and La Niña and IOZM are coincidental, and that El Niño and La Niña does not necessarily predispose the IO to, or initiate, IOZM events. While Webster et al. (1999) agreed with Saji et al. (1999) that the IOZM involves relatively independent mechanisms, they explored the possibility that the El Niño and La Niña may initiate or positively reinforce IOZM events. They examined the extreme 1997 positive IOZM event, and suggested that it was unusually strong and persistent because of interactions with a simultaneous strong El Niño event. Their rational was that the anomalously warm SSTs over the western IO moistened air that penetrated the African continent resulting in increased convection. The convection amplified the low-level easterly flow and further warmed the western IO via Ekman downwelling. This then strengthened the SST gradient and enhanced precipitation.

The net result was a positive feedback process, with the El Niño event and IOZM event functioning in tandem. While they maintained that the IOZM can be independent of El Niño and La Niña (as evidenced by the many IOZM years without an El Niño event), the strong El Niño and IOZM event that year may have worked in concert to produce the unusually long lasting and intense IOZM event.

Several additional studies closely examined the individual and combined effects of the

IOZM and El Niño and La Niña on SSTs and precipitation patterns in the IO and the HOA (Yamagata et al. 2002; Ashock et al. 2003; Black et al. 2003; Behera et al. 2004). Using composites from multiple observational datasets, Yamagata et al. (2002) documented distinctive SST patterns associated with all IOZM events, pure positive IOZM events, all El Niño events, and pure El Niño events. They almost completely discounted the influence of El Niño, contending that El Niño events were only associated with significantly warmed SSTs when concurrent with positive IOZM events. Ashock et al. (2003) statistically examined and compared values of the NINO3 SST index and the DMI to determine the relative contributions of El Niño and La Niña and IOZM to the zonal equatorial wind anomalies in the IO that force precipitation anomalies in east Africa and the western IO.

They found the DMI to be well correlated with the wind anomalies, while NINO3 is not, suggesting independence of the IOZM from El Niño and La Niña processes. Walker circulation anomalies during pure IOZM events were found to be distinctly different from those during pure El Niño events. The convective branch of the Walker circulation, usually located over central Africa, exhibited a clear shift toward east Africa during pure IOZM events, while changes in this convection were diffuse and inconsistent during El Niño events. Behera et al. (2004) evaluated 41 years of observational data and a 200-year run of a coupled, atmosphere-ocean general circulation model to determine underlying causes for east African short rains variability.

They found that most precipitation variability is associated with the IOZM; that the IOZMs influence is overwhelming when compared to that of ENSO; and that the correlation between El Niño /Southern oscillation(ENSO) and the east African short rains is insignificant when the influence of the IOZM is excluded.

Their model simulation supported the findings of earlier studies we discussed with respect to the basic structure and evolution of the characteristic IOZM features (e.g., anomalies in winds, SSTs, etc.) prior to, during, and after anomalous short rains events. Changes

to the mean location of the ascending branch of the Walker circulation, forced by SST anomalies initiated during IOZM events led to anomalous moisture transport into, and enhanced convection over, east Africa.

Black et al. (2003) concluded that strong El Niño/ La Niña forcing can predispose the atmosphere-ocean system in the IO region to an IOZM event and is, therefore, a contributing factor in extreme eastern African rainfall.

They contended that the IOZM and El Niño and La Niña should not be viewed in isolation from one another. Their rationale is that the observed net impact of El Niño/La Niña on east African rainfall is a result of complex alignment and interplay among several climate factors. They highlight the inconsistencies in the El Niño and La Niña response by pointing out that African rains were enhanced during three very strong El Niño events (1972, 1982, and 1997), but they also found that rainfall can be below average during weaker El Niño events (1969, 1976, 1986, 1987, and 1991). And, they point out that the IOZM is inconsistent as well; it is only during extreme IOZM events that east African rainfall is systematically affected.

Consistent with Saji et al. (1999), Yamagata et al. (2002), Ashok et al. (2003), and the early work by Hastenrath et al. (1993), Black et al. (2003) concluded that the most important mechanism for extreme rainfall during positive IOZM events seems to be a weakening of the climatological low level westerlies over the north-central IO and a strong anomalous SST dipole in the tropical IO with positive (negative) SSTAs in the western (eastern) IO. This results in reduced moisture transport away from east Africa and enhanced short rains. Black et al. (2003) contended that dynamical explanations are essential when dealing with this highly complex, situation.

The mechanisms for precipitation variability in east Africa are apparently highly nonlinear, and cannot be explained well by even the most sophisticated statistical methods. This contention is reinforced by the weak correlations they found between the DMI and east African rainfall, and between the SOI and east African rainfall.

Chapter 4

TRANSFORMATIONS OF MOIST AIR

Water may exist in a solid, liquid or gaseous phase depending upon temperature and pressure. The terms evaporation and condensation are used to describe water in transition between the gaseous and liquid phases. A saturation state is a state of equilibrium between water molecules in transition between the liquid phase and gaseous phases. The temperatures and pressures at which saturation states occur are of great importance in determining the course of most weather-related phenomena. As we will see, water vapor, while a very small component of the atmosphere (percentage wise), plays a huge role in determining the course of weather and climate.

Winds enhance evaporation by transporting water vapor molecules in the air away from the site where the water is entering the air, preventing the air from becoming saturated at that site. Higher temperatures also enhance evaporation.

Water molecules in the liquid and gaseous states exist in a state of rapid motion, zipping back and forth as a result of their relatively high energy and collisions with other water molecules. In a parcel of water at a given temperature there will be a distribution of energies associated with various water molecules (i.e., not all of the water molecules will possess the same energy). The higher the temperature the higher the mean value of the energy distribution or the higher the average energy of each water molecule. The greater the energy of an individual water molecule the more vigorous its motion. Water molecules

at higher energies move around with greater average speeds (rms speeds).

Whenever water exists in the liquid state there will be at least a few molecules that have high enough energies to make the transition from the liquid to the vapor state. When the air is warm, however, many water vapor molecules will possess high enough energies to bounce around for only a short period of time before escaping the liquid state. When the air is cooled, however, lower rms speeds allow water molecules to stick to certain objects (known as condensation nuclei) after a collision. When water sticks to condensation nuclei in the air, liquid cloud droplets begin to form. Condensation is more likely when the air is cooled both because water vapor molecules can stick to condensation nuclei, and because lower rms speeds allow more water vapor molecules to return to the liquid state.

4.1 Circulation of Water in the Atmosphere

The transfer of water between land, ocean and atmosphere is accomplished by a number of natural processes. Evaporation places water into the atmosphere. Transpiration, the transfer of water into the atmosphere by biological systems (primarily plants), also places water into the atmosphere.

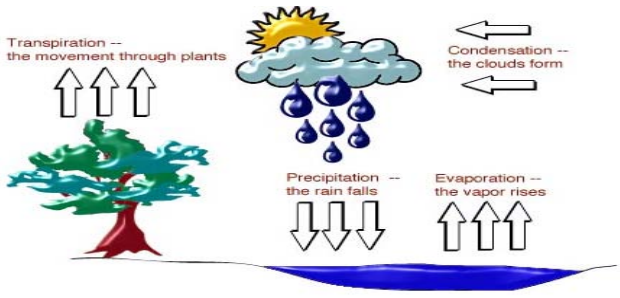

Figure 4.1: Circulation of water in the atmosphere

Evaporation and transpiration work together in continental areas and account for

roughly 15 percent of the total amount of water placed into the atmosphere. The other 85 percent comes directly from the oceans via evaporation.

4.1.1 Humidity

The amount of water vapor in the air is referred to as humidity. Humidity may be usefully defined in any of several ways. Absolute humidity is equal to the mass of water vapor divided by the total volume of air, or water vapor density. Absolute humidity changes as the volume of an air parcel changes. Changes in the volume of an air parcel occur normally as air rises or sinks.

Specific humidity is equal to the mass of water vapor in the air divided by the total mass of the air parcel (including the water vapor). Since this is a unitless number, it is expressed as a percentage. A relative humidity of 100 percent means that an air parcel is completely saturated. It is important to note that it is entirely possible to have relative humidity greater than 100 percent. It is, in fact, necessary for relative humidity to exceed 100 percent for certain meteorological processes to occur. Although adding or removing water vapor from the air will bring about changes in relative humidity, this is not the only way that such changes can occur. A change in temperature of the air can also change the relative humidity.

Dew Point is the temperature to which a parcel of air must be cooled, at constant pressure and water vapor content, for saturation to occur. Dew point is determined with respect to a flat surface of water. The corresponding frost point is determined with respect to a flat surface of ice. Dew point is a very useful indicator of the airs actual water vapor content. High dew points correspond to high water vapor content. When air temperature and dew point are far apart relative humidity is low. When air temperature and dew point are close together relative humidity is high.

In the atmosphere, variability within regions comparable to the size of a model grid cell

often results in saturated areas where clouds exist and subsaturated areas where clouds are not present. When the saturated fraction of the region is small, so is the cloud fraction, and vice versa. Thus one would expect that there is a direct link between the average grid cell relative humidity (among other variables) and the cloud fraction as well as the cloud water content. The subgrid explicit moisture scheme (SUBEX) accounts for the subgrid variability observed in nature by linking the average grid cell relative humidity to the cloud fraction and cloud water following the work of Sundqvist et al. (1989). SUBEX includes simple formulations for raindrop accretion and evaporation.

Additional modifications are in the specification of the autoconversion threshold. These modifications improve the physical manner in which large-scale clouds and precipitation are represented with little computational sacrifice. In this approach, each model grid cell is divided into a clear and cloud portion. Any variable V is the average of the values in the clear and cloudy portions of the grid cell, V_{nc}, and V_c, respectively, weighted by fractional cloud (FC), by the following relationship:

$$V = FC.V_c + (1 - FC)\, V_{nc} \tag{4.1.1}$$

where FC fractional cloud at a given model level varies based on the average grid cell relative humidity RH according to the following relation:

$$FC = \left(\frac{RH - RH_{min}}{RH_{max} - RH_{min}} \right)^{\frac{1}{2}} \tag{4.1.2}$$

where RH_{min} is the relative humidity threshold at which clouds begin to form, and RH_{max} is the relative humidity where FC reaches unity. FC is assumed to be zero when RH is less than RH_{min} and unity when RH is greater than RH_{max}.

RH_{min} are associated with greater subgrid variability. Typical values for RH_{min} range from 60 to 100 percent depending on a variety of factors, including the vertical level

[Sundqvist, 1988], the surface characteristics (Sundqvist et al., 1989), and the model resolution. The threshold over land is often specified lower than the threshold over ocean due to sub-grid-scale surface heterogeneities that translate upward into the atmosphere (Sundqvist et al.,1989). These heterogeneities can result from variable topography, soil moisture, vegetation, surface friction, etc. The ocean surface is relatively homogeneous in that the surface roughness is small and temperatures do not vary considerably at small scales. Sundqvist et al. (1989) use 75 and 85 percent for land and ocean, respectively. Within the boundary layer and at lower temperatures (238 K), they let RH_{min} increase linearly to a value near unity. Preliminary experiments varying RHmin by $\mp$5 percent resulted in negligible changes.

Pricipitation P is described as follows when the cloud water content exceeds the autoconvsersion threshold Q_c^{th} according to:

$$P = C_{ppt}(\frac{Q_c}{FC} - Q_c^{th})FC \tag{4.1.3}$$

$\frac{1}{C_{ppt}}$ can be considered as the characteristics time for cloud droplets conversion to rain drops. For simplicity RH_{min} is set at 80 percent for land and 90 percent for ocean and the default setting not allow RH_{min} to vary in the vertical or with temperature. RH_{max} is also to 1.01, allowing water vapor content to exceed the saturation value by 1 percent. The autoconversion threshold Q_c^{th} is based on the analysis of Gultepe and Isaac (1997). They used aircraft observations of cloud liquid water content and related them to temperature. Here the threshold is obtained by scaling the median cloud liquid water content equation according to the following:

$$Q_c^{th} = C_{acs}10^{-0.49+0.013T} \tag{4.1.4}$$

where T is temperature in degrees Celsius, and C_{acs} is the autoconversion scale factor. By

scaling the Q_c temperature relationship, we assume that the threshold takes the shape of the mean cloud conditions. Over the ocean there are typically fewer cloud condensation nuclei than over land. As a result, the cloud droplets over the ocean are larger and hence less buoyant than those over land [Rogers and Yau, 1989]. Larger cloud droplets tend to result in more collision and coalescence. Thus continental clouds tend to be thicker than maritime clouds for the same probability of precipitation (Rogers and Yau, 1989).

4.1.2 Raindrop Accretion

Raindrop accretion can be an important process under certain climatic conditions (Rogers and Yau, 1989). The cloud water in excess of the autoconversion threshold is allowed to precipitate out. Thus when clouds form, they often linger at or near the autoconversion threshold (in the absence of other atmospheric processes such as cloud evaporation). In nature, however, when precipitation initiates (exceeds the autoconversion threshold), rain droplets falling through clouds collect and remove a portion of the cloud droplets. Thus neglecting this process can result in an underprediction of precipitation and overprediction of clouds, particularly in humid regions. Accounting for it allows the cloud water content to fall below the autoconversion threshold when precipitation occurs. SUBEX includes a simple formulation for the accretion cloud droplets by falling rain droplets according to the following relation based on Beheng (1994):

$$P_{acc} = C_{acc} Q_c P_{sum} \tag{4.1.5}$$

where P_{acc} is the amount of accreted cloud water, C_{acc} is the accretion rate coefficient, and P_{sum} is the accumulated precipitation from above falling through the cloud. Accretion only takes place in the cloudy portions of the grid cell. For simplicity, P_{sum} is assumed to be distributed uniformly across the grid cell. In other words, no knowledge of the

cloud fraction in which the precipitation formed is used. In some cases, this may tend to overestimate the effects of accretion.

4.1.3 Raindrop Evaporation

Raindrop evaporation can also be an important process under certain conditions (Rogers and Yau, 1989). In arid regions, a significant quantity of the precipitation that forms often evaporates before it reaches the surface. Neglecting this process may lead to the simulation of excessive precipitation in arid regions (Small et al., 1999a). SUBEX employs the simple formulation of Sundqvist et al. (1989) as follows:

$$P_{evap} = C_{evap}\,(1 - RH)\,P_{sum}^{\frac{1}{2}} \tag{4.1.6}$$

where P_{evap} is the raindrop evaporation and C_{evap} is the evaporation rate coefficient.

Chapter 5

CLIMATE OF ETHIOPIA

Ethiopia makes up the greater part of the East African. At latitudes of 4^0 to 15^0N, Ethiopia's climate is typically tropical in the southeastern and northeastern lowland regions, but much cooler in the large central highland regions of the country. Mean annual temperatures are around 15–20^0C in these high altitude regions, while 25–30^0C in the lowlands. Seasonal rainfall in Ethiopia is driven mainly by the migration of the Inter Tropical Convergence Zone (ITCZ). The exact position of the ITCZ changes over the course of the year, oscillating across the equator from its northern most position over northern Ethiopia in July and August, to its southern most position over southern Kenya in January and February. Most of Ethiopia experiences one main wet season (called Kiremt) from mid June to mid September (up to 350mm per month in the wettest regions), when the ITCZ is at its northernmost position. Parts of northern and central Ethiopia also have a secondary wet season of sporadic, and considerably lesser, rainfall from February to May (called the Belg). The southern regions of Ethiopia experience two distinct wet seasons which occur as the ITCZ passes through this more southern position. The March to May Belg season is the main rainfall season yielding 100–200mm per month, followed by a lesser rainfall season in October to December called Bega (around 100mm per month). The eastern most corner of Ethiopia receives very little rainfall at any time of year. The

movements of the ITCZ are sensitive to variations in Indian Ocean sea surface temperatures and vary from year to year, hence the onset and duration of the rainfall seasons vary considerably inter annually, causing frequent drought. The most well documented cause of this variability is the El Niño Southern Oscillation (ENSO). Warm phases of ENSO (El Niño) have been associated with reduced rainfall in the main wet season, JAS, in north and central Ethiopia causing severe drought and famine, but also with enhanced rainfalls in the earlier February to April rainfall season which mainly affects southern Ethiopia.

5.1 SEASONS AND SEASONAL CLASSIFICATIONS

In high and mid-latitudes, seasons are classified as winter, spring, summer and autumn, while in low latitudes they are categorized as wet and dry seasons. In the case of Ethiopia, the seasons are classified into three periods based on annual rainfall patterns. Hence, based on the mean annual and mean monthly rainfall distributions, the rainfall regimes are delineated and the types of seasons in Ethiopia are identified.

The central and most of the eastern half of the country has two rainy periods and one dry period. The two rainy periods are locally known as Kiremt (June to September) and Belg (February to May), which are long and short rainy periods, respectively. The annual rainfall distribution over this region shows two peaks corresponding to the two rainy seasons, separated by a relatively short "dry" period. The dry period, which covers the rest of the year (i.e., October to January), is known as Bega.

The western part of Ethiopia, has one rainfall peak during the year. As one goes toward the north within this region, the length of the rainy period (June to September) decreases due to the meridional migration of the ITCZ (Inter-Tropical Convergence Zone).

The southern and the southeastern parts of Ethiopia have two distinct dry periods (December to February and June to August). The temporal distribution of rainfall over these regions shows two distinct peaks separated by a well-marked dry period.

However, for southwestern, western, central and northwestern Ethiopia only one dry and one long rainy season can be identified. Thus, the presence of four seasons, notably, winter (December- February), spring (March-May), summer (June-August) and autumn (September–November) are evident.

5.2 Weather System Affecting Ethiopia

Seasonal and annual rainfall variations in Ethiopia as well as the neighboring areas of the region are associated with the macro-scale pressure systems and monsoon flows (Tesfaye 1986, 1987; Hastenrath, 1991). Bekuretsion(1987) has indicated that the weather and climate of Ethiopia arises from the influence of tropical weather systems, like the Intertropical Convergence Zone (ITCZ), the monsoon, easterly waves, etc., and quasi-stationary subtropical anticyclones of both northern and southern hemisphere. The interactions between the tropical and extratropical weather systems produce major active weather over the country, especially during the months of February to May (Northern Hemisphere Spring). The main weather bearing systems for the Bega, Belg and Kiremt seasons, respectively are discussed below.

During Bega (the dry season) the country predominantly falls under the influence of warm and cool northeasterly winds. These dry air masses originate either from the Saharan anticyclone or from the ridge of high pressure extending into Arabia from the large high over central Asia (Siberia). However, occasionally the northeasterly winds are interrupted when migrating low pressure systems originating in the Mediterranean area move southwards and interact with the tropical systems resulting unseasonal rains over central and northern Ethiopia. Occasionally the development of the Red Sea Convergence Zone (RSCZ) also produces rains over northeastern Ethiopia (Pedgley, 1966).

During Belg (the small rainy season) which is from March to May, the Arabian high moves

towards the northern Arabian Sea. When it is pushed over the water body, it causes a moist southeasterly air current to flow towards Ethiopia (Camberlin et al, 2002; NMSA 1996).

Occasionally, there are also frontal lows that either originate from the Mediterranean area or originate within the Atlantic Ocean and are swept through from west to east. These occur in association with a cold front, the intensity of which depends on the temperature contrast ahead and behind the front. As it reaches east of Mediterranean Sea, the surface front is split into two: one front over the Arabian lowland and the other over the Sudan lowland (Gizaw, 1968).

5.2.1 Atlantic Ocean

The decline of rainfall in eastern, south and south-western Ethiopia over the period approximately from 1986 to 2002 is related to the corresponding persistent warming of the South Atlantic Ocean.

The sea-surface temperature (SST) over the tropical eastern Pacific Ocean is not significantly correlated with the main rainfall of the semi-arid lowland areas of eastern, southern, and southwestern Ethiopia, except at marginal zones in transition to the Ethiopian Highlands(Sileshi and Zanke, 2004).

5.2.2 Indean Ocean

The variability of African rainfall is statistically related to both Pacific and Indian oceans, but the variability in the two oceans is also related. While the SST variability of the tropical Pacific exerts some influence over the African region, it is the atmospheric response to the Indian Ocean variability that is essential for simulating the correct rainfall response over eastern, central, and southern Africa. Analysis of the dynamical response(s) seen in the numerical experiments and in the observations indicate that the Pacific and Indian

Ocean have a competing influence over the Indian Ocean/African region.

This competition is related to the influence of the two oceans on the Walker circulation and the consequences of that variability on low-level fluxes of moisture over central and southern Africa (Hastenrath and Polzin, 2003).

Comparison of the wind anomalies that develop during extreme Indian Ocean dipole or Zonal mode (IOZM) events with those that develop during weaker (moderate) events shows that strong easterly anomalies in the northern-central Indian ocean are a persistent feature of extreme, but not of moderate, IOZM years. It is suggested that these anomalies weaken the westerly flow that normally transports moisture away from the African continent, out over the Indian Ocean. Thus, during extreme IOZM years, rainfall is enhanced over east Africa and reduced in the central and eastern Indian Ocean basin.

It is also shown that the IOZM cannot be viewed in isolation from the ENSO. Instead it is postulated that in some years, a strong ENSO forcing can predispose the Indian Ocean coupled system to an IOZM event and is therefore a contributory factor in extreme East African rainfall. The results of this study imply that the relationship between El Niño and the IOZM explains the previously described association between El Niño and high East African rainfall. Thus, understanding the way that ENSO drives Indian Ocean dynamics may aid the development of predictive scenarios for East African climate that could have significant economic implications (Emily and Julia, 2002).

Over the last few decades, the Indian Ocean has warmed by over 1K which resulted in a weakening of the large scale Indian monsoon circulation because of the reduction in land sea temperature contrast.

Chapter 6

REGIONAL CLIMATE MODELING

Climate varies across a wide range of temporal and spatial scales. Yet, climate modeling has long been approached using global models that can model only the broad scales of at mospheric circulations and their interaction with convective cells, land, ocean circulation, and other environmental variables. An alternative to global modeling is regional climate modeling. As the name implies, a regional climate model (RegCM) does not attempt to simulate the entire globe but only a small portion.

6.1 RegCM4

The Regional Climate Model system (RegCM4), originally developed at the National Center for Atmospheric Research (NCAR), is maintained in the Earth System Physics (ESP) section of the International Centre for Theoretical Physics (ICTP). The first version of the model, RegCM1, was developed in 1989 and since then it has undergone major updates in 1993 (RegCM2), 1999 (RegCM2.5), 2006 (RegCM3) and most recently 2010

(RegCM4). The latest version of the model, RegCM4, is now fully supported by the ESP, while previous versions are no longer available. This version includes major upgrades in the structure of the code and its pre and post processors, along with the inclusion of some new physics parameterizations. The model is flexible, portable and easy to use. It can be applied to any region of the World, with grid spacing of up to about 10 km (hydrostatic limit), and for a wide range of studies, from process studies to paleoclimate and future climate simulation.

Model improvements currently under way include the development of a tropical band version, coupling with a regional ocean model, inclusion of full gas phase chemistry, upgrades of some schemes (convection, PBL, cloud microphysics) and development of a non-hydrostatic dynamical core.

6.2 The RegCM Model Horizontal and Vertical Grid

It is useful to first introduce the models grid configuration. The modeling system usually gets and analyzes its data on pressure surfaces, but these have to be interpolated to the models vertical coordinate before input to the model. The vertical coordinate is terrain following meaning that the lower grid levels follow the terrain while the upper surface is flatter. Intermediate levels progressively flatten as the pressure decreases toward the top of the model. A dimensionless δ coordinate is used to define the model levels as in the following equation where p is the pressure, p_t is a specified constant top pressure, p_s is the surface pressure:

$$\delta = \frac{(P - P_t)}{(P_s - p_t)} \tag{6.2.1}$$

δ is zero at the top and one at the surface, and each model level is defined by a value of δ. The model vertical resolution is defined by a list of values between zero and one that do not necessarily have to be evenly spaced.

6.3 Map Projections and Map Scale Factors

The modeling system has a choice of four map projections. Lambert Conformal is suitable for midlatitudes, Polar Stereographic for high latitudes, Normal Mercator for low latitudes, and Rotated Mercator for extra choice. The x and y directions in the model do not correspond to west-east and north-south except for the Normal Mercator projection, and therefore the observed wind generally has to be rotated to the model grid, and the model u and v components need to be rotated before comparison with observations. These transformations are accounted for in the model pre-processors that provide data on the model grid. The map scale factor, m, is defined by

m = (distance on grid)/ (actual distance on earth)

and its value is usually close to one, varying with latitude. The projections in the model preserve the shape of small areas, so that dx=dy everywhere, but the grid length varies across the domain to allow a representation of a spherical surface on a plane surface. Map scale factors need to be accounted for in the model equations wherever horizontal gradients are used.

6.4 Dynamics

The model dynamic equations and numerical discretization are described by Grell et al. (1994). Horizontal Momentum Equations are

$$\begin{aligned}\frac{\partial P^* u}{\partial t} &= -m^2\left(\frac{\partial P^* \frac{uu}{m}}{\partial x} + \frac{\partial P^* \frac{vu}{m}}{\partial y}\right) - \frac{\partial P^* u\dot{\sigma}}{\partial \sigma} - mP^*\left[\frac{RT_v}{\frac{(P^*+p_t)}{\sigma}}\frac{\partial P^*}{\partial x} + \frac{\partial \phi}{\partial x}\right] \\ &\quad + fP^* v + F_H u + F_v u, \end{aligned} \tag{6.4.1}$$

$$\frac{\partial P^* v}{\partial t} = -m^2\left(\frac{\partial P^* \frac{uv}{m}}{\partial x} + \frac{\partial P^* \frac{vv}{m}}{\partial y}\right) - \frac{\partial P^* v\dot{\sigma}}{\partial \sigma} - mP^*\left[\frac{RT_v}{\frac{(P^*+p_t)}{\sigma}}\frac{\partial P^*}{\partial y} + \frac{\partial \phi}{\partial y}\right] + fP^* u + F_H v + F_v v, \tag{6.4.2}$$

where u and v are the eastward and northward components of velocity, T_v is virtual temperature, ϕ is geopotential height, f is the coriolis parameter, R is the gas constant for dry air, m is the map scale factor for either the Polar Stereographic, Lambert Conformal, or Mercator map projections, $\dot{\sigma} = \frac{\partial \dot{\sigma}}{\partial t}$, and F_H and F_V represent the effects of horizontal and vertical diffusion, and $p^* = p_s$ - p_t.

Continuity and Sigmadot ($\dot{\sigma}$) Equations are

$$\frac{\partial P^*}{\partial t} = \frac{\partial P^* \frac{u}{m}}{\partial x} + \frac{\partial P^* \frac{v}{m}}{\partial y} - \frac{\partial P^* \dot{\sigma}}{\partial \sigma} \tag{6.4.3}$$

The vertical integral of Eq (6.4.2) is used to compute the temporal variation of the surface pressure in the model,

$$\frac{\partial P^* v}{\partial t} = -m^2 \int_0^1 \left(\frac{\partial P^* \frac{u}{m}}{\partial x} + \frac{\partial P^* \frac{v}{m}}{\partial y}\right) d\sigma' \tag{6.4.4}$$

After calculation of the surface pressure tendecy, $\frac{\partial P^*}{\partial t}$ the vertical velocity in sigma coordinates ($\dot{\sigma}$) is completed at each level in the model from the vertical integral

$$\dot{\sigma} = -\frac{1}{P^*}\int_0^\sigma \left[\frac{\partial P^* v}{\partial t} + m^2\left(\frac{\partial P^* \frac{u}{m}}{\partial x} + \frac{\partial P^* \frac{v}{m}}{\partial y}\right)\right] d\sigma' \tag{6.4.5}$$

where σ' is a dummy variable of integration and $\dot{\sigma}(\sigma = 0) = 0$.

The thermodynamic equation is

$$\frac{\partial P^* T}{\partial t} = -m^2\left(\frac{\partial P^* \frac{uT}{m}}{\partial x} + \frac{\partial P^* \frac{vT}{m}}{\partial y}\right) - \frac{\partial P^* T\dot{\sigma}}{\partial \sigma} + \frac{RT_v\omega}{C_{pm}\left(\frac{\sigma+P_t}{P_{ast}}\right)} + \frac{P^* Q}{C_{pm}} + F_H T + F_v T, \tag{6.4.6}$$

where C_{pm} is the specific heat for moist air at constant pressure, Q is the diabatic heating, $F_H T$ represents the horizontal diffusion, $F_v T$ represents the effect of vertical mixing and dry convective adjustment, and the vertical velocity is

$$\omega = P^* \dot{\sigma} + \sigma \frac{\partial P^*}{\partial t}, \tag{6.4.7}$$

where,

$$\frac{\partial P^*}{\partial t} = \frac{\partial P^*}{\partial t} + m(u \frac{\partial P^*}{\partial x} + v \frac{\partial P^*}{\partial y}) \tag{6.4.8}$$

the expression for $C_{pm} = C_p(1 + 0.8q_v)$, C_p is the specific heat at constant pressure for dry air and q_v is the mixing ratio of water vapour.

The hydrostatic equation is used to compute the geopotential heights from the virtual temperature T_v,

$$\frac{\partial \phi}{\partial \ln(\sigma + \frac{P_t}{P^*})} = -RT_v[1 + \frac{q_c + q_r}{1 + q_v}]^{-1} \tag{6.4.9}$$

where $T_v = T(1 + 0.608q_v)$, q_v, q_c, and q_r are the water vapor, cloud water or ice, and rain water or snow, mixing ratios.

6.5 Physics

6.5.1 Radiation Scheme

RegCM4 uses the radiation scheme of the NCAR CCM3, which is described in Kiehl et al. (1996). The solar component, which accounts for the effect of O_3, H_2O, CO_2, and O_2, follows the -Eddington approximation of Kiehl et al. (1996). The cloud scattering and absorption parameterization follow that of Slingo (1989), whereby the optical properties of the cloud droplets (extinction optical depth, single scattering albedo, and asymmetry parameter) are expressed in terms of the cloud liquid water content and an effective droplet radius.

When cumulus clouds are formed, the gridpoint fractional cloud cover is such that the

total cover for the column extending from the model computed cloud-base level to the cloud top level (calculated assuming random overlap) is a function of horizontal gridpoint spacing. The thickness of the cloud layer is assumed to be equal to that of the model layer, and a different cloud water content is specified for middle and low clouds.

6.5.2 Land Surface Models

Biosphere-Atmosphere Transfer Scheme (BATS) is a surface package designed to describe the role of vegetation and interactive soil moisture in modifying the surface atmosphere exchanges of momentum, energy, and water vapor.

Sensible heat, water vapor, and momentum fluxes at the surface are calculated using a standard surface drag coefficient formulation based on surface layer similarity theory. The drag coefficient depends on the surface roughness length and on the atmospheric stability in the surface layer.

The surface evapotranspiration rates depend on the availability of soil water. BATS has 20 vegetation types sand, loam, clay, and different soil colors for the soil albedo calculations.

6.5.3 Planetary Boundary Layer Scheme

The planetary boundary layer scheme, developed by Holtslag et al. (1990), is based on a nonlocal diffusion concept that takes into account countergradient fluxes resulting from large scale eddies in an unstable, well mixed atmosphere. The vertical eddy flux within the PBL is given by

$$F_c = -K_c(\frac{\partial C}{\partial z} - \gamma_c) \tag{6.5.1}$$

where γ_c is a countergradient trasport term describing nonlocal transport due to dry deep convection, K_c is the eddy diffusion, and C is the eddy flux of property in the z direction.

6.5.4 Convective Precipitation Schemes

There are about four convective precipitation parameterizationm schemes. In this work, the Grell scheme is used. The description of Grell scheme is as outlined below.

The Grell scheme considers clouds as two steady state circulations: an updraft and a downdraft Grell (1993). No direct mixing occurs between the cloudy air and the environmental air except at the top and bottom of the circulations. The mass flux is constant with height and no entrainment or detrainment occurs along the cloud edges. The originating levels of the updraft and downdraft are given by the levels of maximum and minimum moist static energy, respectively. The Grell scheme is activated when a lifted parcel attains moist convection. Condensation in the updraft is calculated by lifting a saturated parcel. The downdraft mass flux (m_o) depends on the updraft mass flux (m_b) according to the following relation:

$$m_o = \frac{\beta I_1}{I_2} m_b \tag{6.5.2}$$

where I_1 is the normalized updraft condensation, I_2 is the normalized downdraft evaporation, and β is the fraction of updraft condensation that re-evaporates in the downdraft. β is the depends on the wind shear and typically varies between 0.3 and 0.5. Rainfall is given by

$$P^{CU} = I_1 m_b (1 - \beta) \tag{6.5.3}$$

Heating and moistening in the Grell scheme are determined both by the mass fluxes and the detrainment at the cloud top and bottom. In addition, the cooling effect of moist downdrafts is included. Due to the simplistic nature of the Grell scheme, several closure assumptions can be adopted. RegCM4 earlier version directly implements the quasi-equilibrium assumption of Arakawa Schubert (AS74). It assumes that convective clouds

stabilize the environment as fast as non-convective processes destabilize it as follows:

$$m_b = \frac{ABE'' - ABE}{NA\Delta t} \tag{6.5.4}$$

where ABE is the buoyant energy available for convection, ABE'' is the amount of buoyant energy available for convection in addition to the buoyant energy generated by some of the non-convective processes during the time interval buoyant t, and NA is the rate of change of ABE per unit m_b. The difference $ABE'' - ABE$ can be thought of as the rate of destabilization over time Δt. ABE'' is computed from the current fields plus the future tendencies resulting from the advection of heat and moisture and the dry adiabatic adjustment. In the latest RegCM4 version, by default, we use a stability based closure assumption, the FC80 type closure assumption, that is commonly implemented in GCMs and RCMs. In this closure, it is assumed that convection removes the ABE over a given time scale as follows:

$$m_b = \frac{ABE}{NA\tau} \tag{6.5.5}$$

where τ is the ABE removal time scale. The fundamental difference between the two assumptions is that the AS74 closure assumption relates the convective fluxes and rainfall to the tendencies in the state of the atmosphere, while the FC80 closure assumption relates the convective fluxes to the degree of instability in the atmosphere. Both schemes achieve a statistical equilibrium between convection and the large scale processes.

Chapter 7

DATA AND METHODOLOGY

7.1 Experimental Setup

In this study sensitivity runs were performed for fourteen moisture scheme parameters resulting in total eighty four runs. The sensitivity of models runs of five upto eight sets of experiments for each individual SUBEX parameters of the subgrid explicit moisture processes are done. This include bottom model level with no clouds (ncld), autoconversion rate for the land and ocean (qland and qoce), autoconversion threshold (Q_c^{th}) for the land and ocean (guland, guloce), minimum relative humidity over the land and ocean (rhland, rhoce), maximum relative humidity (rh_{max}), maximum cloud cover (fc_{max}), effect of temperature (tc0) on SUBEX, rain drop evaporation rate coefficient (C_{evap}), Cloud liquid water content for convective precipitation (cllwcv), Max cloud fractional cover for convective precipitation ($clfrcv_{max}$) and rain drop accretion rate (C_{accr}) are varied within the allowed physical limits such that the defualt settings are enclosed within the variations for the normal year of summer 2000.

ERA-Interim data set is used for initial conditions (ICs) and exponential lateral boundary conditions (LBCs) during sensitivity runs of each of the fourteen parameters as well as long year runs using defualt and new set of parameters. Sea surface temperature from

optical interpolation weekly (OI-WK) are used as surface boundary conditions. For the ICs and LBCs quantities each reanalysis dataset is interpolated to the grid of the RegCM4 and the first set of interpolation fields is used as ICs for the simulation. The physics of convective precipitation scheme used in this experiment is a Grell Arakawa –Schubert (Grell AS) scheme. The RegCM4 was run with the same horizontal resolution of 60km and 18 vertical levels. The domain is 39.9^0 to west and 80.44^0 degree in the East direction and from 24.6^0 to south and 25.1^0 North direction as shown in Fig.7.1.

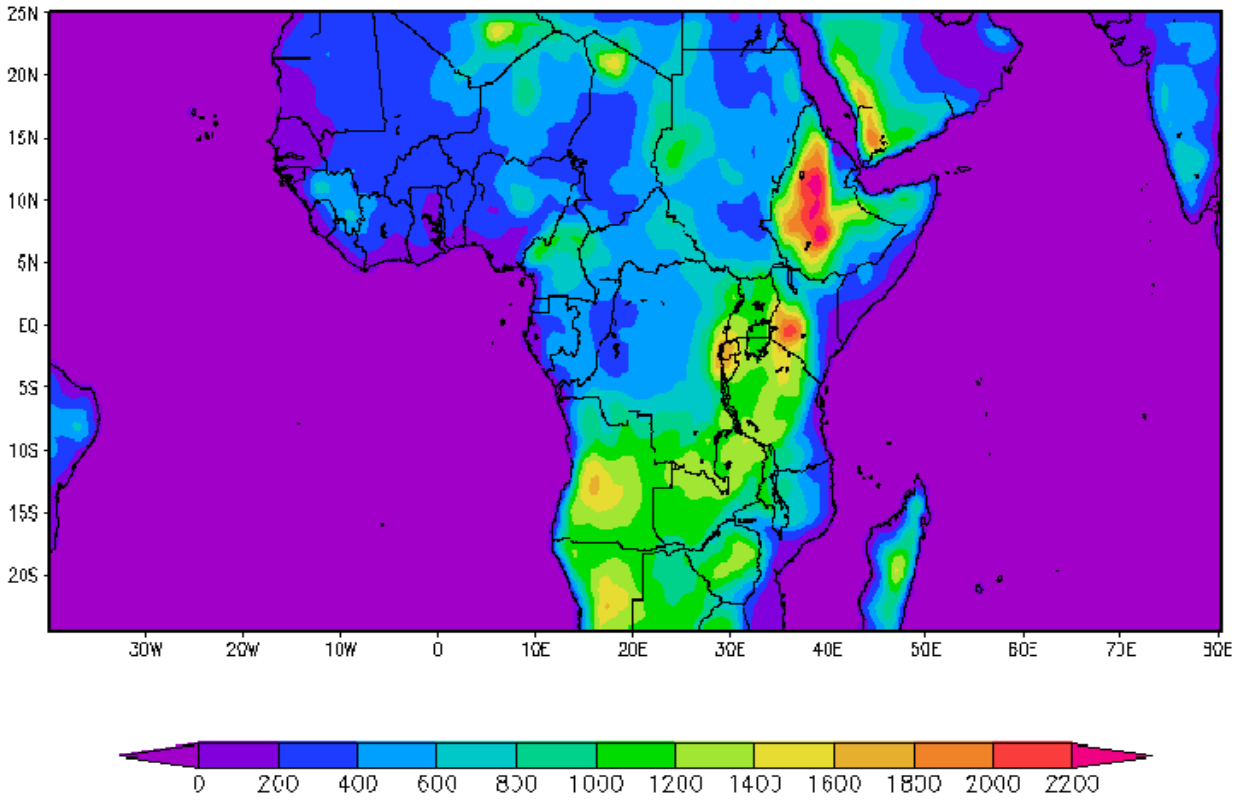

Figure 7.1: RegCM4 Simulation Domain

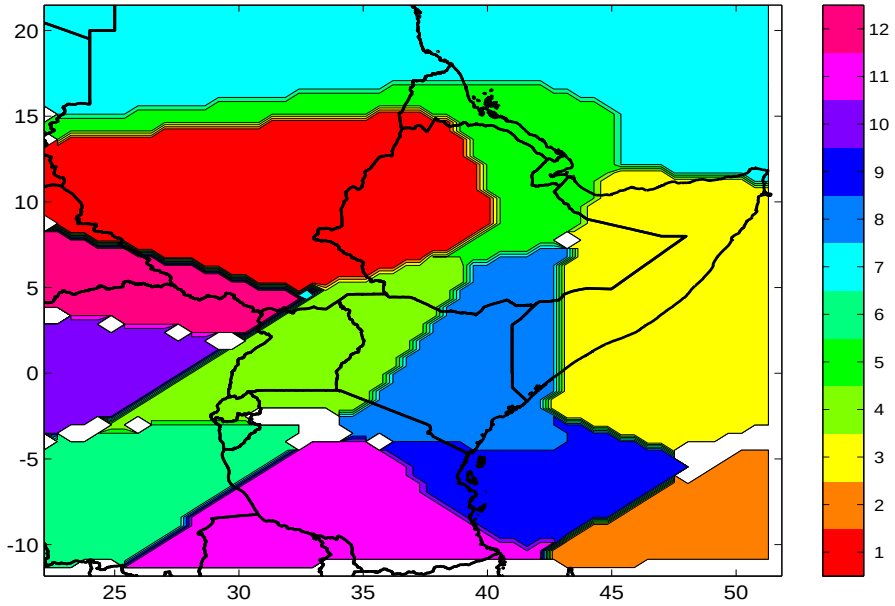

Figure 7.2: Delineated regions

7.2 Boundary conditions

7.2.1 Surface boundary conditions

Orography is incorporated in the model as the lower boundary condition in a terrain following vertical coordinate system. Pressure has been widely used as a vertical coordinate in modeling and theoretical studies. There are however deficiencies of the sigma treatment of orography. This scheme may not handle sharp terrain gradients effectively. The orography data used in this study was taken from the global 2.5^0 horizontal resolution orography file archived at International Research Institute (IRI). This data was interpolated to the model horizontal grid resolution of 60km using the linear interpolation scheme. The land-use data adopted in the model was interpolated from 2.5^0 resolution data archived at National Centers for Atmospheric Research (NCAR). The time dependent SST was interpolated from a $1^0 X 1^0$ grid of the monthly mean observed data. The

surface pressure, air temperature, humidity are some of surface boundary condition variables.

7.2.2 Lateral boundary and initial conditions

This scheme consists of Newtonian and diffusion terms that gradually drive the model solution of wind components, temperature, water vapor mixing ratio, and surface pressure toward specified large scale values inside the lateral buffer zone. The lateral boundary condition variables are:

- Wind;
- Temperature;
- Water vapor; and
- Surface pressure.

As the size of the horizontal domain decreases, the specification of the velocity components and temperature along the boundaries affects the mean values of these quantities over the entire domain to an ever increasing degree. Thus, on a domain of 224×96, a set of boundary conditions may be computationally stable and produce smooth results, but even small errors in the treatment of precipitation, temperature or velocity may profoundly affect the mean kinetic and internal energy budgets over the domain.

Initial conditions in a numerical simulation represent the mean space time characteristics of the atmosphere at the beginning of the numerical experiment. The fields for both lateral and initial conditions are obtained ECMWF reanalysis. After completion of ERA-40, effort was devoted to development of a new reanalysis system derived from the latest version of the operational European Center for Medium Range Weather Forecast (ECMWF) system. In 2006 a new reanalysis was started from January 1989, to produce an interim

reanalysis (ERA-Interim) for the data rich 1990s and 2000s, to be continued as ECMWF Climate Data Assimilation System (ECDAS) until superseded by a new extended reanalysis.

The main advances of the ERA-Interim data assimilation over the ERA-40 system are: 12 hour 4D Var, T255 horizontal resolution, better formulation of background error constraint, new humidity analysis, improved model physics, quality control of data drawing on experience from ERA-40 and variational bias correction of satellite radiance data, improvements in radiosonde temperature and surface pressure bias handling, more extensive use of radiances, improved fast radiative transfer model and assimilation of rain affected Sea Surface Model (SSM) radiances through 1D-Var.

ERA-Interim uses mostly the observations prepared for ERA-40 supplemented by data for later years from ECMWFs operational archive. Boundary forcing fields are taken from ERA-40 until 2002, and from ECMWF operations for later dates. However a few new dataset have been acquired. The ERA-INTERIM is a reanalysis of the global atmosphere covering the data rich period since 1989, and continuing in real time. As ERA-Interim continues forward in time, updates of the Archive will take place on a monthly basis.

The ERA-INTERIM project was initiated in 2006 to provide a bridge between ECMWFs previous reanalysis, ERA-40 (1957-2002), and the next generation extended reanalysis envisaged at ECMWF. The main objectives of the project were to improve on certain key aspects of ERA-40, such as the representation of the hydrological cycle, the quality of the stratospheric circulation, and the handling of biases and changes in the observing system. These objectives have been largely achieved as a result of a combination of factors, including many model improvements, the use of 4-dimensional variational analysis, a revised humidity analysis, the use of variational bias correction for satellite data, and other improvements in data handling.

The atmospheric model is coupled to an ocean-wave model resolving 30 wave frequencies and 24 wave directions at the nodes of its reduced one-degree latitude/longitude grid.

The main characteristics of the ERA-Interim system and many aspects of its performance are described in ECMWF.

7.3 Validation Data Set: CMAP and GPCP Precipitation

In this study, RegCM4 Pricipitation is compaired with Global Precipitation Climatology Project (GPCP) and CPC Merged Analysis of precipitation (CMAP). Rain-gauge measurement is the traditional and oldest method for monitoring rainfall. However, because of practical observational limitations it suffers from numerous gaps in space and time, thus often making its use in climate diagnostic studies less reliable. On the other hand, rainfall estimates based on satellites is spatially and temporally comprehensive when calibrated using rain-gauge measurements (Xie and Arkin 1995). Xie and Arkin (1997) produced a global precipitation data set called CMAP to assist in problems encountered when relying just on rain-gauge observations. CMAP is a global precipitation data set that uses a global $2.5^0 \times 2.5^0$ grid resolution, temporally distributed monthly/pentad from January 1979 - present.

The Global Precipitation Climatology Project (GPCP) Monthly Precipitation Analysis is globally complete, monthly analysis of surface precipitation at $2.5^0 \times 2.5^0$ latitude-longitude resolution is available from January 1979 to the present. It is a merged analysis that incorporates precipitation estimates from low orbit satellite microwave data, geosynchronous orbit satellite infrared data, and surface rain gauge observations. The merging approach utilizes the higher accuracy of the low orbit microwave observations to calibrate, or adjust, the more frequent geosynchronous infrared observations.The dataset is extended back into the premicrowave era (before mid-1987) by using infrared-only observations calibrated to the microwave based analysis of the later years. The combined satellite based product is adjusted by the rain gauge analysis. The dataset archive also contains the

individual input fields, a combined satellite estimate, and error estimates for each field. This monthly analysis is the foundation for the GPCP suite of products, including those at finer temporal resolution. The 23-yr GPCP climatology is characterized, along with time and space variations of precipitation.

7.4 Correlation, RMSE and Bias

The performance of RegCM4 over different part of Horn of African region for rainfall pattern during 1989-2008 simulation period is determined by analysis of the correlation, the root mean square error (RMSE), bias, of the simulated and observed precipitation.

Simple correlation analysis can be used to determine the degree of linear relationship between the RegCM4 precipitation and the observational precipitation over Ethiopia. For any month k, simple correlation coefficient r_k between the RegCM4 precipitation, M and observational precipitation, O can be expressed as

$$r_k = \frac{\sum_{k=1}^{N}(M_k - M')(O_K - O')}{[(\sum_{k=1}^{N}(M_k - M')^2(\sum_{k=1}^{N}(O_k - O')^2)]^{\frac{1}{2}}} \tag{7.4.1}$$

where N is the total number of records, M' and O' are a long term mean of RegCM4 and observation, respectively. The value of r_k is between -1 and 1. positive and negative values of r_k are indicative of the positive or negative relationships, respectively.

Root mean square error ($RMSE$) is a measure of the square difference between the RegCM4 simulated precipitation and observed precipitation values at each cluster (grid point). If ppt^M and ppt^O are the RegCM4 and observed field the $RMSE$ can be estimated using the relationship

$$RMSE = [\frac{\sum_{i=1}^{N}(ppt^M - ppt^O)^2}{N}]^{\frac{1}{2}} \tag{7.4.2}$$

where the simulation is carried out over N grid points in a predefined region and the superscripts M and O refers to model and observation. The model performance is evaluated

by comparing the mean simulated rainfall with the corresponding observational rainfall pattern. Systematic $RMSE$ represents the error that is similar at all points in the gridded data. Accurate models have low systematic $RMSE$.

The bias is a time average of the error defined as:

$$Bias = \frac{\sum_{i=1}^{N}(ppt^M - ppt^O)}{N} \tag{7.4.3}$$

Chapter 8

RESULTS AND DISCUSSION

A total of eighty four model runs during sensitivity model runs and two additional model experiments for long period to assess the improvement in simulation of precipitation based on new set of SUBEX parameters versus the defualt setting are performed. In the following section, we consider both sensitivity studies and long year run.

8.1 Sensitivity Studies for Moisture Scheme Parameters

Table 8.1 shows sensitivity studies accomplished for 14 SUBEX variables The first row shows the model runs which includes the defualt and additional runs of upto seven expirements while the first coloumn shows the SUBEX variables. The improvement in precipitation prediction (if any) based on the new values of the parameters is evaluated using correlation, RMSE and bias of RegCM4 with corresponding CMAP and GPCP values.

subex param-eters	default	run1	run2	run3	run4	run5	run6	run7
$ncld$	1	0	2	3	4			
fc_{max}	0.80	0.50	0.60	0.70	0.90	1.00		
$qland$	$0.25E^{-3}$	$0.5E^{-4}$	$0.15E^{-3}$	$0.5E^{-3}$	$0.75E^{-3}$	$0.1E^{-2}$	$0.5E^{-2}$	$0.1E^{-1}$
$qoce$	$0.25E^{-3}$	$0.5E^{-4}$	$0.15E^{-3}$	$0.5E^{-3}$	$0.75E^{-3}$	$0.1E^{-2}$	$0.5E^{-2}$	$0.1E^{-1}$
$guland$	0.4	0.3	0.5	0.6	0.7	0.8		
$guloce$	0.4	0.3	0.35	0.45	0.5	0.55		
rh_{max}	1.01	0.80	0.85	0.90	0.95	1.00	1.03	1.05
$rhland$	0.80	0.65	0.70	0.75	0.85	0.95		
$rhoce$	0.90	0.70	0.75	0.85	0.90	0.95		
$tc0$	238.0	230	234	242	246	250	260	270
$caccr$	3	1	2	4	5	6		
$cevap$	$.100E^{-2}$	$0.35E^{-2}$	0.50^{-2}	0.60^{-2}	$0.75E^{-2}$	$0.85E^{-2}$		
$cllwcv$	$0.3E^{-3}$	$0.1E^{-3}$	$0.2E^{-3}$	$0.4E^{-3}$	0.5^{-3}	0.6^{-3}		
$clfrcv_{max}$	0.25	0.15	0.20	0.35	0.40	0.45		

Table 8.1: Sensitivity expirements based on JJAS runs of the normal year of 2000.

Fig.8.1 shows correlation of RegCM4 precipitation for different values of rain drop accretion rate with CMAP and GPCP precipitation. The new values of accretion rate donot improve the simulation of precipitation for all the 12 homogeneous regions identified in the Horn of Africa regions. Instead, the defualt values of 0.3 performs better than the new values interms of performance measures such as correlation as well as RMSE and bias.

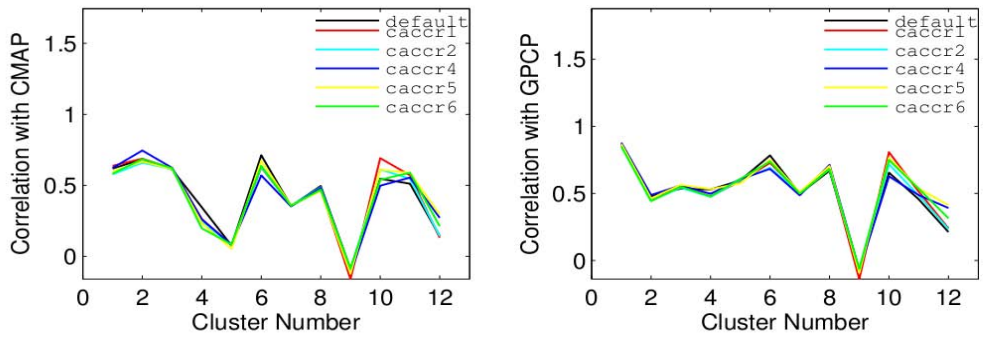

Figure 8.1: Correlation of simulated precipitation with CMAP (left panel) and GPCP (right) for different values of rain drop accretion rate

The rain drop evaporation rate is varied as shown in Table 8.1. This parameters needs to be suitably adjusted to avoid excessive rainfall in arid regions. Fig. 8.2 shows the correlation simulated of precipitation for different values of rain drop evaporation rate with CMAP (left panel) and GPCP (right panel). Eventhough the sensivity to this parameter is not as such significant the performance of the new value of 0.75×10^{-2} is relatively good compaired to the default values as well as the other values using the test runs for the majority of clusters in the region. This is also evident from precipitation bias with respect CMAP and GPCP (not shown) which exhibit smaller bias over cluster 2–8 and 10–12.

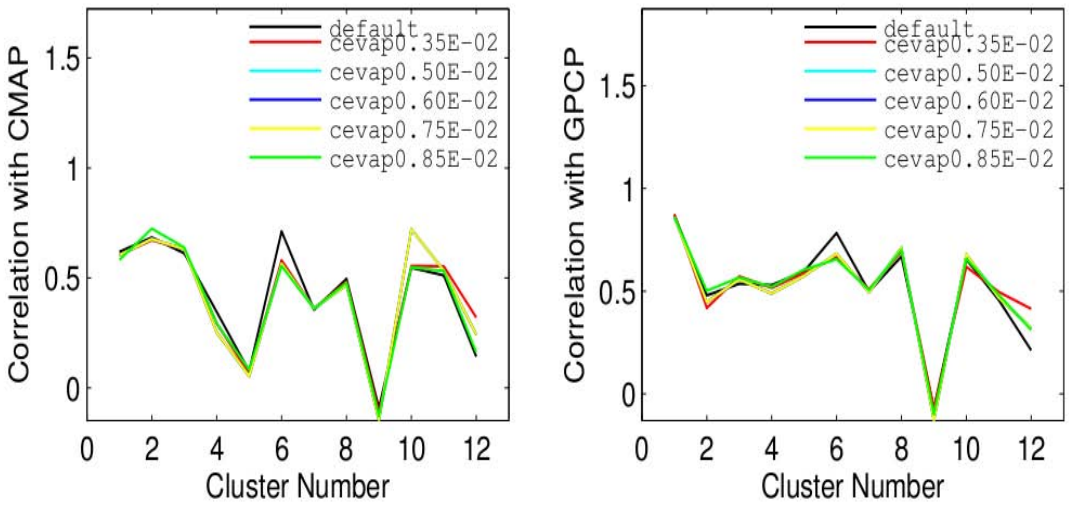

Figure 8.2: Correlation of simulated precipitation with CMAP (left panel) and GPCP (right panel) for different values of rain drop evaporation rate.

In the atmoshere variability within regions comparable to the size of a model grid cell often results in saturated areas where cloud exist and subsaturated area where clouds are not present. When the saturated fraction of the region is small so is the cloud fraction and vise versa.

Fig. 8.3 shows better sensitivity in fc_{max} than other parameters in SUBEX which is apparent from the scatter for different values of fc_{max}. The values for fc_{max} of 0.50

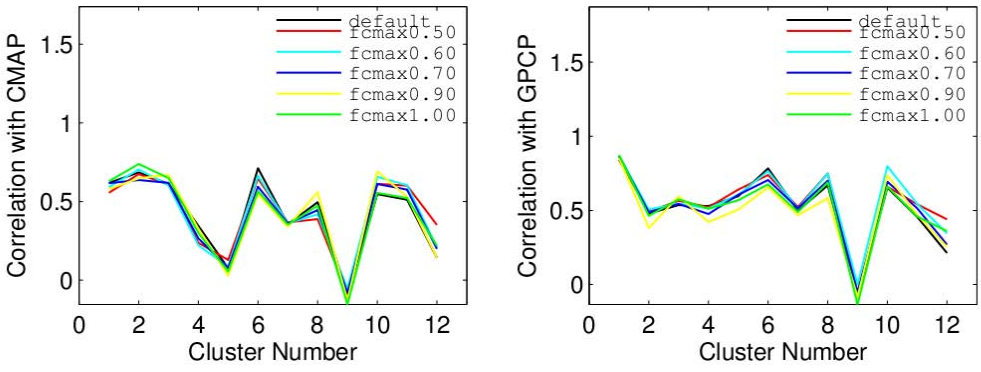

Figure 8.3: Correlation of simulated precipitation with CMAP (left panel) and GPCP (right panel) for different values of maximum cloud fraction (fc_{max}).

shows better correlation with CMAP and GPCP (Fig. 8.3) as well as small RMSE (not shown) and bias (Fig.8.4) over most of the 12 clusters.

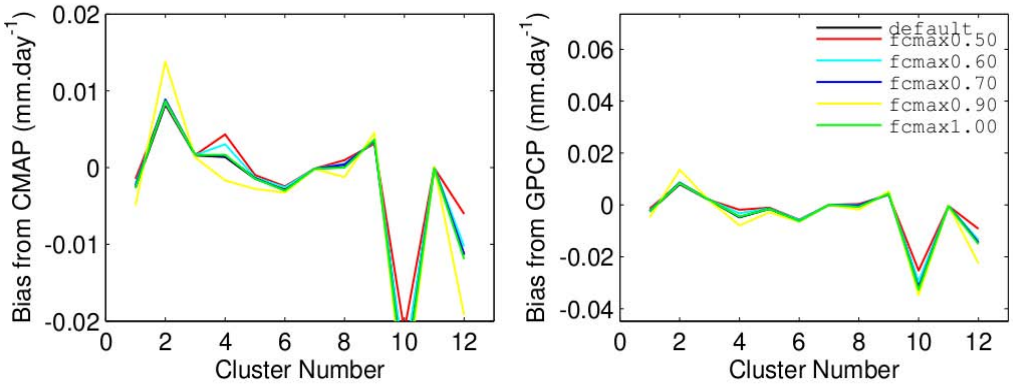

Figure 8.4: Bias of simulated precipitation with respect to CMAP (left panel) and GPCP (right) for different values of maximum cloud fraction (fc_{max}).

The other major change takes place by the subgrid explicit moisture scheme change of autoconversion threshold (Q_c^{th}). It reliad upon of the cloudliquid water temperature relationship. Subgrid explicit moisture scheme is highly sensitive to the autoconversion threshold parameter.

Figs. 8.5 and 8.6 show the autoconversion thresholds for land (guland) and ocean (guloce) respectively. The values of 0.30 and 0.55 for guland and guloce are found to perform better than the default values 0.40 in terms good correlation as well as less RMSE and bias.

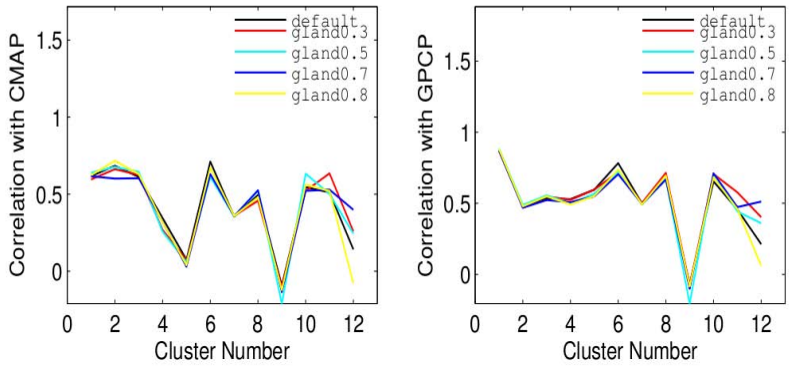

Figure 8.5: Correlation of simulated precipitation with respect to CMAP (left panel) and GPCP (right) for different values of autoconversion threshold over land (guland).

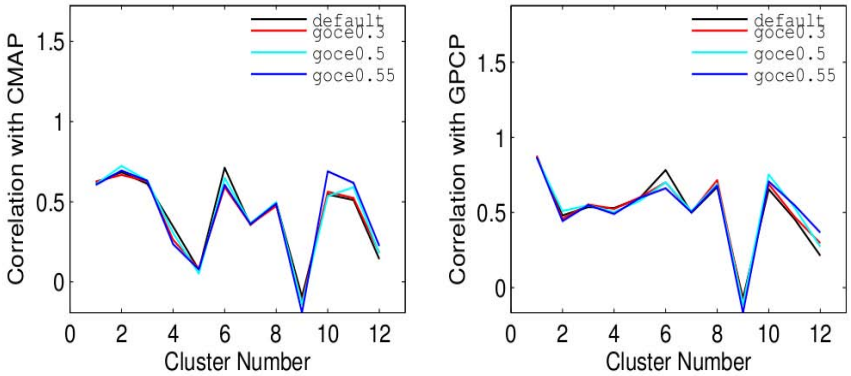

Figure 8.6: Correlation of simulated precipitation with respect to CMAP (left panel) and GPCP (right) for different values of autoconversion threshold over ocean (guloce).

The autoconversion rate sensitivity over land and ocean perform to reduce the stratiform rainfall. Figs. 8.7 and 8.8 show sensitivity of non convective precipitation to autoconversion rate over land (qland) and ocean (qoce) respectively. The value of 0.15×10^{-3} for qland has shown to perform well in capturing the observed precipitation. Similarly, a value of 0.15×10^{-3} for qoce performs better than a default value of 0.25×10^{-3} in reproducing the CMAP and GPCP rainfall.

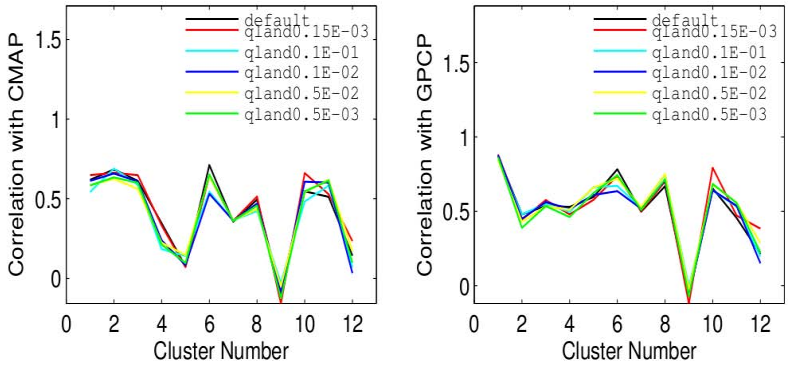

Figure 8.7: Correlation of simulated precipitation with respect to CMAP (left panel) and GPCP (right) for different values of autoconversion rate over land (qland).

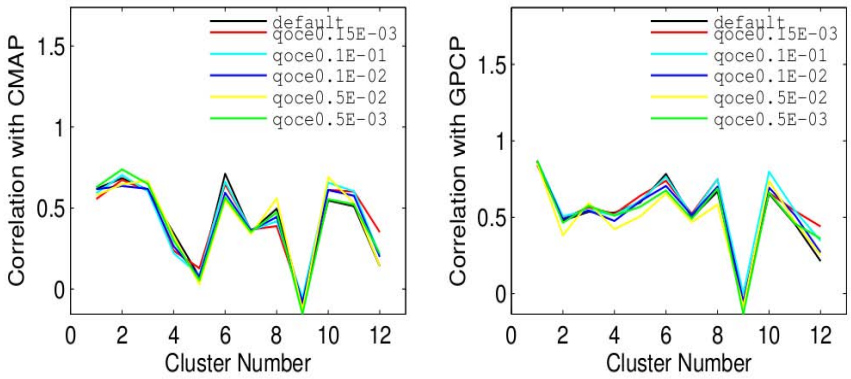

Figure 8.8: Correlation of simulated precipitation with respect to CMAP (left panel) and GPCP (right) for different values of autoconversion rate over ocean (qoce).

The sensitivity of precipitation to relative humidity threshold over land and ocean is

shown in Figs. 8.9 - 8.10. The relative humidity minimum of 0.90 performs better than the default value of 0.80 over land for moist parts of Horn of Africa region in capturing observed rainfall. The optimal value for relative humidity minimum over ocean is found to be 0.95 in terms of correlation of simulated precipitation with observational data set (Fig. 8.10).

The relative humidity reduces the intense stratiform events by either increasing or decreasing relative humidity grid cells (RH_{min}) for the land and ocean surfaces. The higher relative humidity threshold the lower cloud cover at lower RH values, the fewer large scale rain events, thereby reducing the amount of rainfall.

Sensitivity of other SUBEX variables namely rh_{max}, cllwcv, $clfrcv_{max}$ and tc0 are

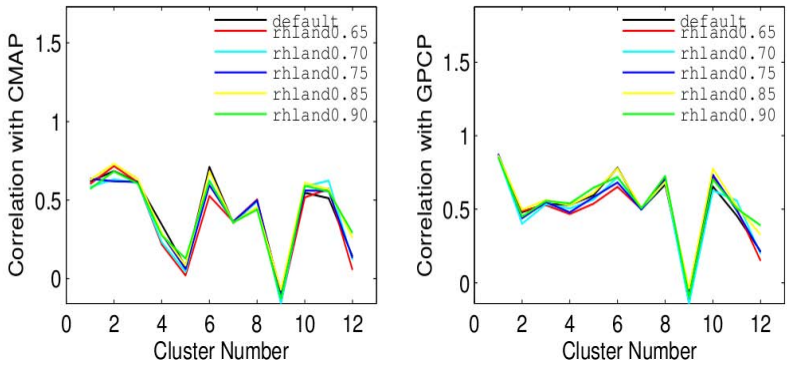

Figure 8.9: Correlation of simulated precipitation with respect to CMAP (left panel) and GPCP (right) for different values of relative humidity minimum over land (rhland).

also performed. rh_{max} and cllwcv do not show any sensitivity in the same manner as accretion rate discussed earlier. However, $clfrc_{max}$ and tc0 are found to capture observed precipitation over most of the clusters if a new value of 0.20 and 246 K are employed (not shown here).

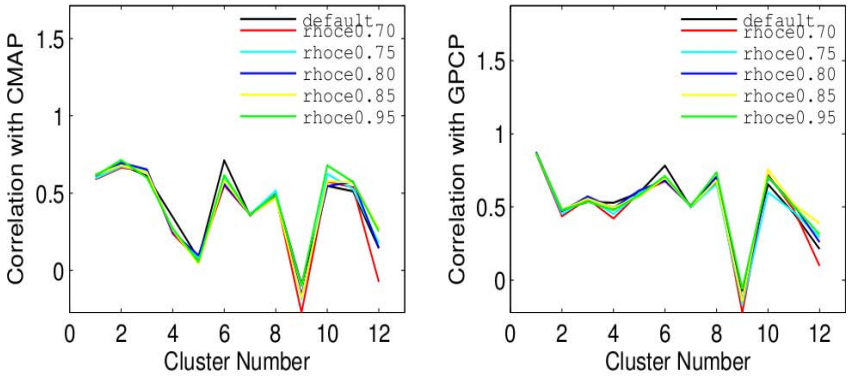

Figure 8.10: Correlation of simulated precipitation with respect to CMAP (left panel) and GPCP (right) for different values of relative humidity minimum over ocean (rhoce).

8.2 Long Years Runs (1989 - 2008) with new set of SUBEX Parameters

This study evaluates the ability of regional climate model (RegCM4) to reproduce the observed rainfall amounts and distribution over the topographically varied region of the Horn of Africa. Using the newly selected SUBEX parameters shown in Table 8.2. The extent of improvement in precipitation simulation with respect old parameter values are also described.

The new parameters of the subgrid explicit moisture scheme (SUBEX) improves the agreement between simulated and observed precipitation for the seasons of the years except that of summer which has high roots mean square error (RMSE) than the default SUBEX parameters and Grell AS convective scheme as shown in Fig. 8.11. Furthermore evaluation of RegCM4 simulation for 1989–2008 shows that the modified moisture scheme (SUBEX) not only reproduce the 19 years average rainfall realistically but also captures interannual variability adequatly over the Horn of Africa.

In RegCM4, both the convective and SUBEX schemes work on subgrid scales however, their approaches are different. The convective schemes try to diagnose if convection will

subex parameter	Perivious values	accepted values from CMAP	Accepted Values from GPCP
$ncld$	1	2	2
fc_{max}	0.80	0.50	0.50
$qland$	$0.25 \exp -3$	$0.1 \exp -1$	$0.1 \exp -1$
$qoce$	$0.25 \exp -3$	$0.15 \exp -3$	$0.15 \exp -3$
$guland$	0.4	0.3	0.3
$guloce$	0.4	0.55	0.55
rh_{max}	1.01	1.01	1.01
$rhland$	0.80	0.90	0.90
$rhoce$	0.90	0.95	0.95
$tc0$	238	246	246
$cevap$	$.100 \exp -2$	$0.75 \exp -2$	$0.75 \exp -2$
$caccr$	3.0	3.0	3.0
$cllwcv$	$0.3 \exp -3$	$0.3 \exp -3$	$0.3 \exp -3$
$clfrcv_{max}$	0.25	0.20	0.20

Table 8.2: New SUBEX parameter values selected based on best performance in capturing CMAP and GPCP precipitation

occur in portions of the grid. This allows them to emulate updrafts in the atmosphere and form precipitation through those updrafts. The large scale precipitation scheme SUBEX does not emulate up drafts, but instead processes the moisture that is already aloft in the atmosphere. In this process it forms clouds and precipitation if critical thresholds of moisture are surpassed.

In RegCM4 the convective scheme is called before the SUBEX scheme. This implies that some SUBEX precipitation could be generated by moisture moved aloft by the convection that moves moisture aloft but that the convective scheme itself does not rain out. Separation of convective and stratiform rain was dependent on which scheme generated the rainfall.

Fig. 8.11 shows correlation of RegCM4 precipitation reproduced using new SUBEX parameters (marked as new) and default (marked as Grell-AS) values shown in Table 8.2 with CMAP(left panel) and GPCP (right panel). There is substantial improvement in reproducing observed precipitation patterns using the new set of SUBEX parameters over

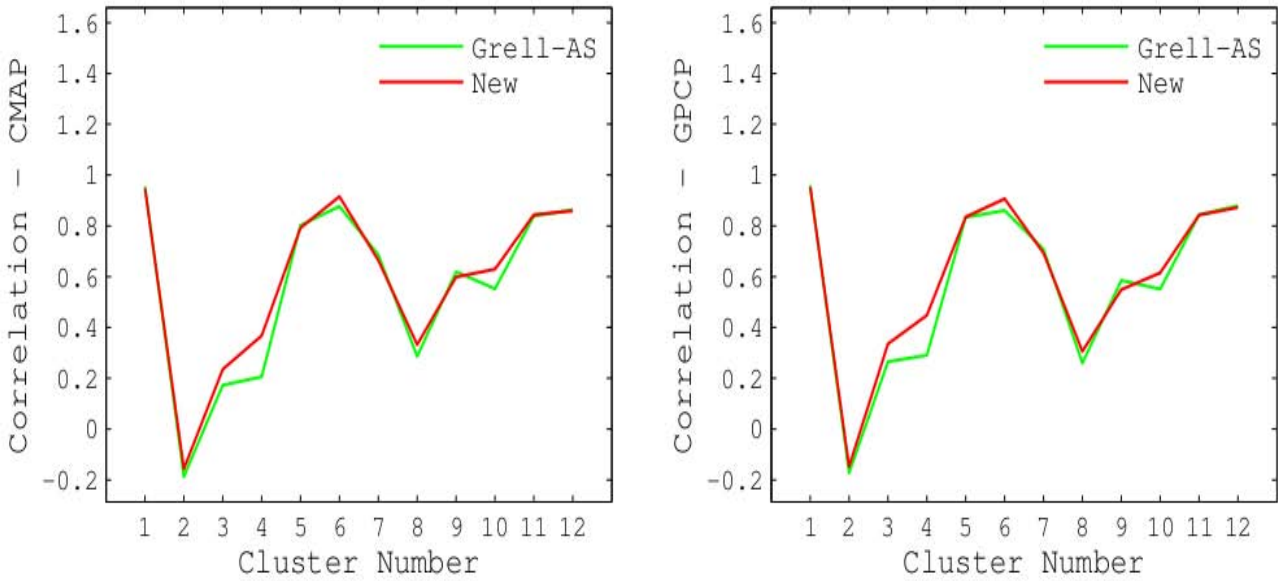

Figure 8.11: Correlation simulated precipitation based on new and old SUBEX with CMAP (left panel) and GPCP (right) for the long year model run.

nearly all clusters. Fig. 8.12 shows corresponding RMSE (upper panels) and bias (lower panels). There is a slight rise in the RMSE over some regions in cluster 6, and 10 - 12. However there is significant improvement in the bias for clusters in the region, especially over the region in cluster 4, 6, 8, 10 - 12.

Fig.8.13 shows the seasonal mean RMSE (top panels) and Bias (bottom panels) of simulated precipitation based on new parameters (red) and old (green) with CMAP (left) and GPCP (right) for the whole Horn of Africa regions. The correlation of the simulated precipitation using new parameters with the observational data set has declined during the JJAS period, which is a wet season for most of northern part of the horn of Africa. From our previous result of cluster analysis, this is probably an artifact introduced due to averaging over the whole domain which is characterized by different seasons. It is considered imperative that RCMs be tested concerning the ability to reproduce historical observations of both mean climate and temporal variability for more extended periods. Therefore, we evaluate the ability of the new SUBEX parameters to reproduce the 1990 -

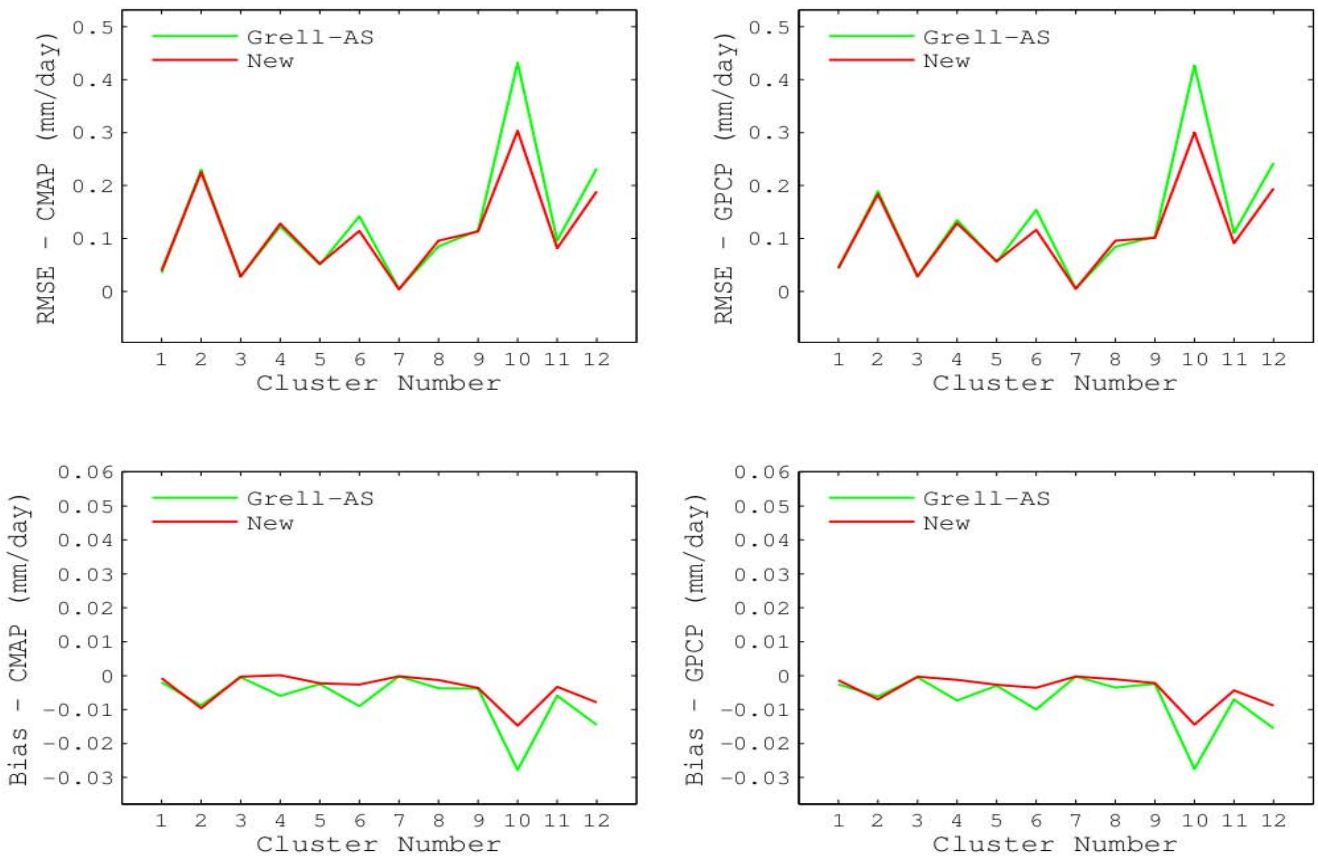

Figure 8.12: RMSE (top) and Bias (bottom) of simulated precipitation based on new and old SUBEX parameters with CMAP (left panel) and GPCP (right) for the long years model run

2008 (19 years) time series for the all the clusters in the region and inter-annual variability within each delineated regions.

The degree of similarity between modelled and observed inter-annual rainfall variability is a valuable model diagnostic that measures the sensitivity moisture schemes over Horn of Africa precipitation. Fig. 8.14 shows remarkable improvement in both magnitude and pattern of precipitation produced using the new parameters. There are several instances at which there is improvement in magnitude which exceeds 2mm/day in contrast to simulation on the basis of defualt values.

Fig. 8.15 shows the 4 time series for cluster 2 which is over Indean Ocean. Both old and new set of parameters have bad performance in capturing the observed pattern as

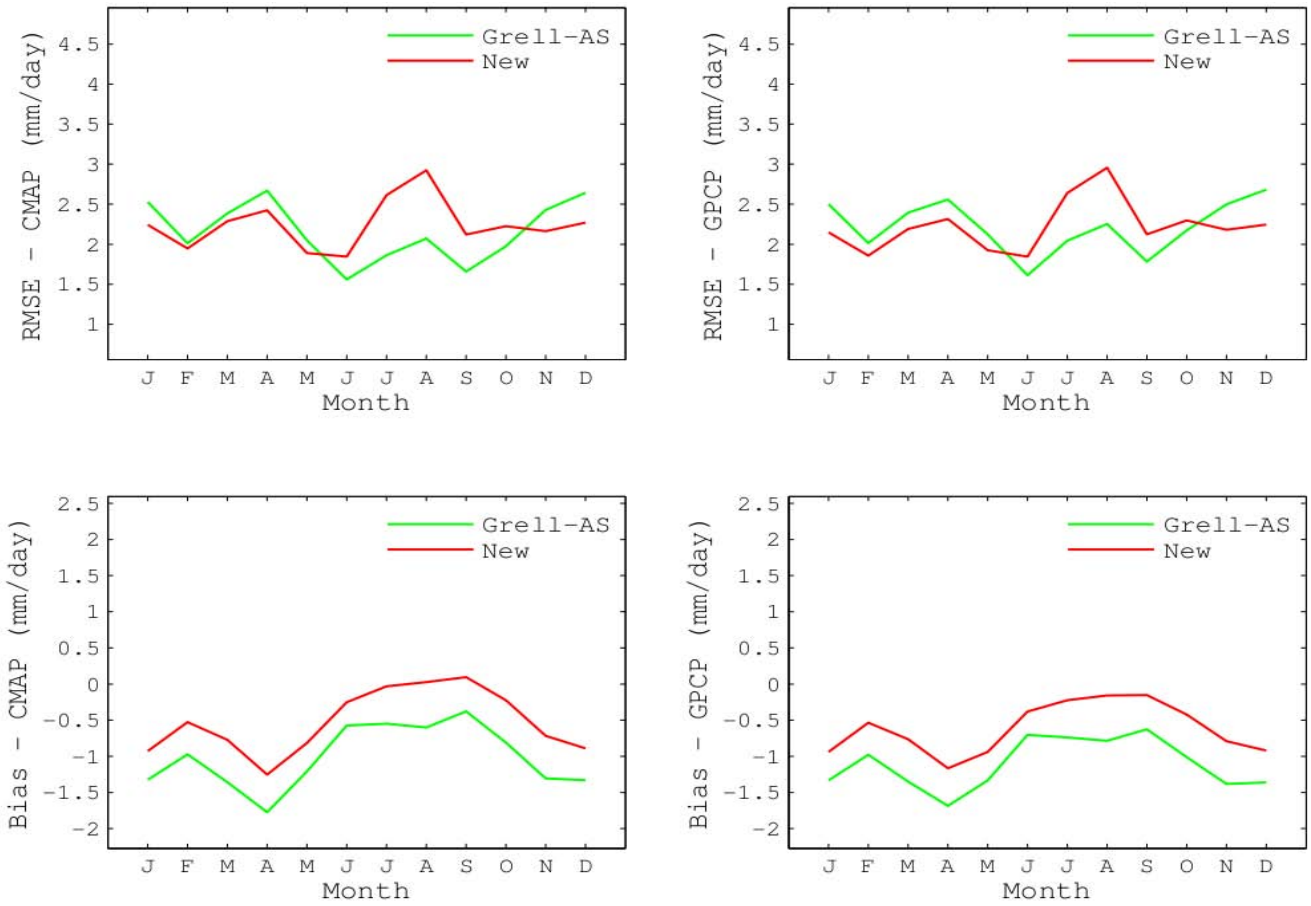

Figure 8.13: RMSE and Bias of simulated precipitation based on new and old SUBEX parameters with CMAP (left panel) and GPCP (right) for the long year model run.

well as magnitudes over the whole simulation period. There is either small or significant over clusters 3, 4, 7, 8, and 9 as shown in Figs. 8.16, 8.17 8.20-8.22. The clusters include regions characterized by low lands, deserts, and semi arid climate. Most of these regions lie in east, northeast, south parts of Horn of Africa, mostly along and towards south and eastern side of the great rift valley. This signals that our choice particularly regarding rain drop evaporation is not optimal. On the otherhand, the new simulation has captured observed inter-annual rainfall variability over clusters 1, 6, 11, 12 remarkably and partly overclusters 5 and 10 as shown in Figs. 8.14, 8.18, 8.19, 8.23 - 8.25. These regions are either on north-western side of great rift valley or south of equator. The north part of Ethiopian main rift valley region is part of the region with moderate improvement.

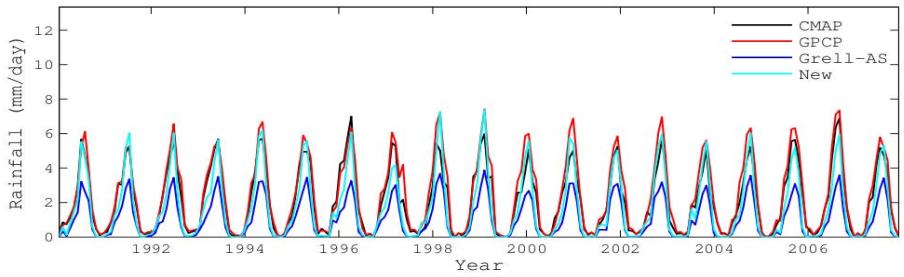

Figure 8.14: Rainfall time series: CMAP (black); GPCP (red); Old SUBEX parameter (marked as Grell-AS, blue); and New parameters (light green) for cluster number-1.

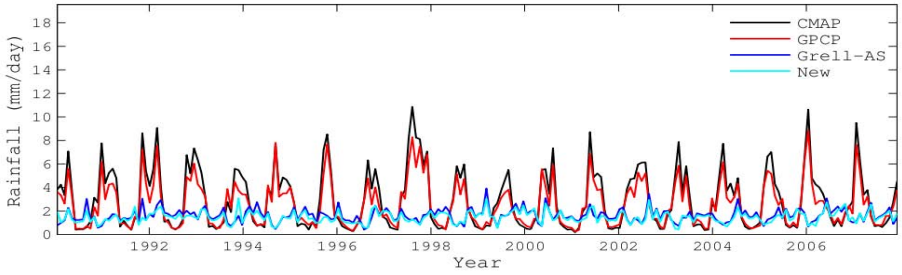

Figure 8.15: Rainfall time series: CMAP (black); GPCP (red); Old SUBEX parameter (marked as Grell-AS, blue); and New parameters (light green) for cluster number-2.

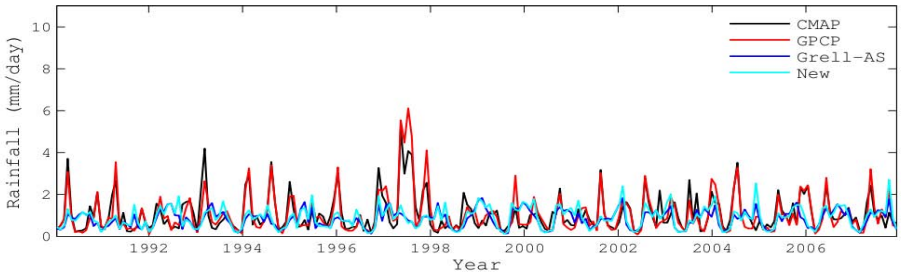

Figure 8.16: Rainfall time series: CMAP (black); GPCP (red); Old SUBEX parameter (marked as Grell-AS, blue); and New parameters (light green) for cluster number-3.

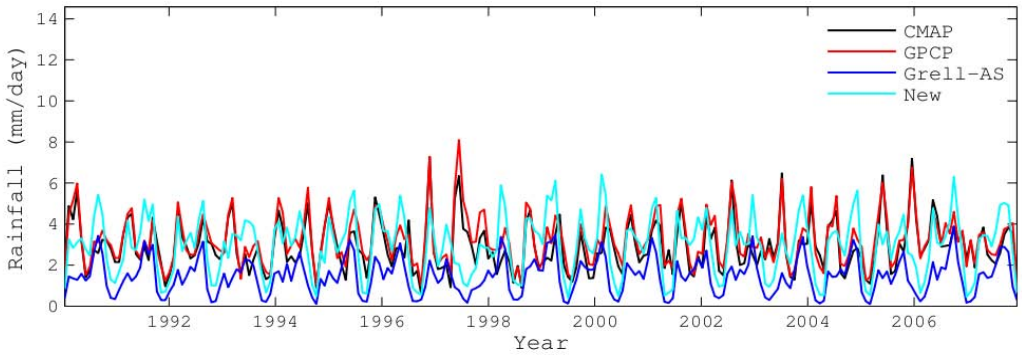

Figure 8.17: Rainfall time series: CMAP (black); GPCP (red); Old SUBEX parameter (marked as Grell-AS, blue); and New parameters (light green) for cluster number-4.

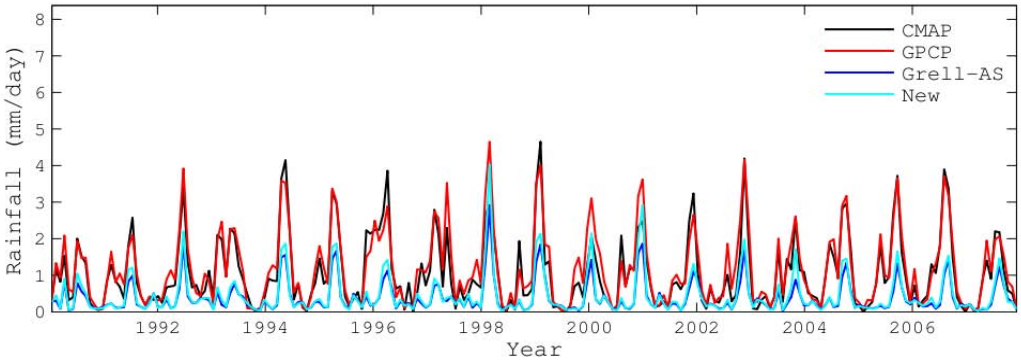

Figure 8.18: Rainfall time series: CMAP (black); GPCP (red); Old SUBEX parameter (marked as Grell-AS, blue); and New parameters (light green) for cluster number-5.

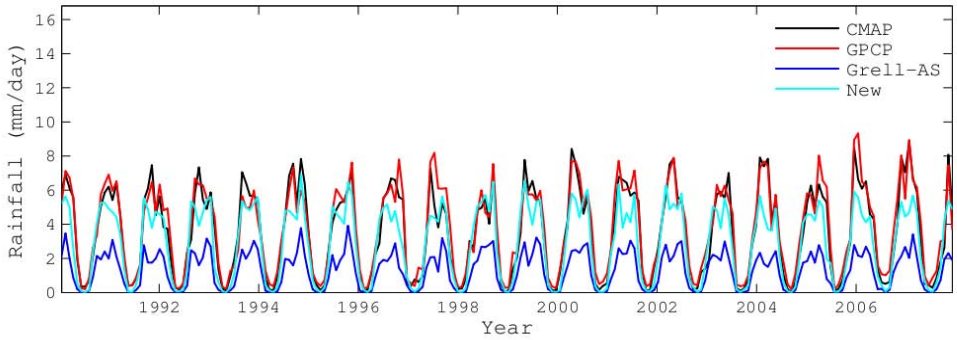

Figure 8.19: Rainfall time series: CMAP (black); GPCP (red); Old SUBEX parameter (marked as Grell-AS, blue); and New parameters (light green) for cluster number-6.

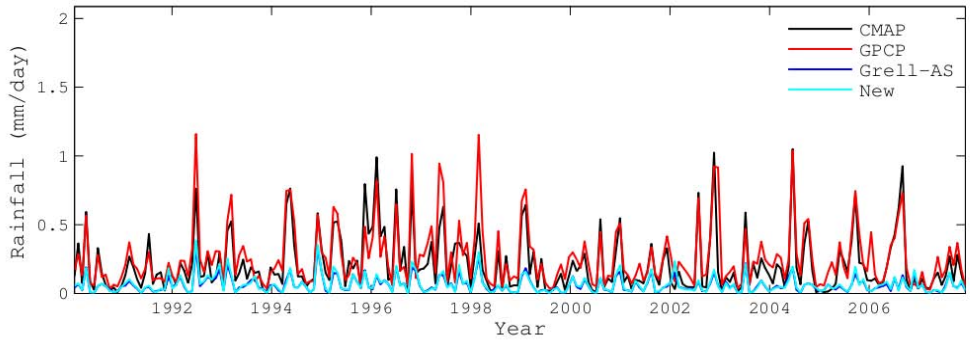

Figure 8.20: Rainfall time series: CMAP (black); GPCP (red); Old SUBEX parameter (marked as Grell-AS, blue); and New parameters (light green) for cluster number-7.

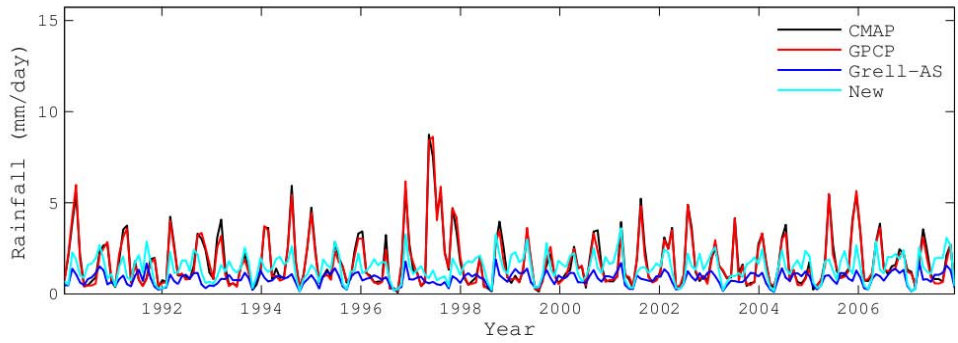

Figure 8.21: Rainfall time series: CMAP (black); GPCP (red); Old SUBEX parameter (marked as Grell-AS, blue); and New parameters (light green) for cluster number-8.

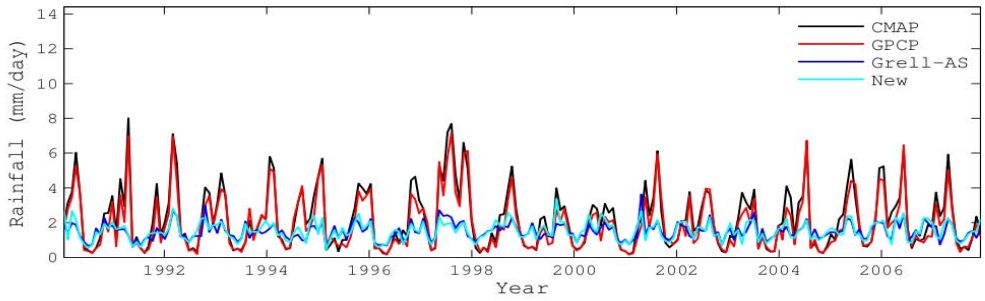

Figure 8.22: Rainfall time series: CMAP (black); GPCP (red); Old SUBEX parameter (marked as Grell-AS, blue); and New parameters (light green) for cluster number-9.

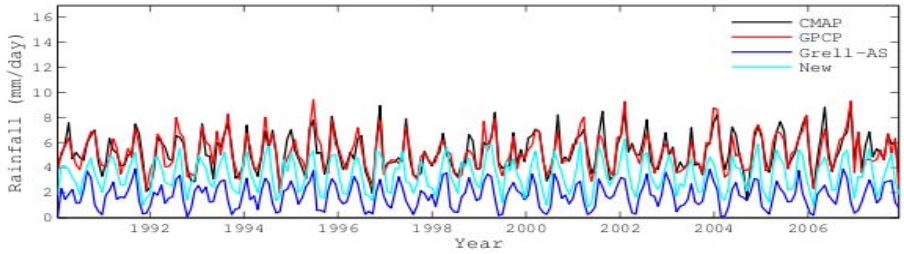

Figure 8.23: Rainfall time series: CMAP (black); GPCP (red); Old SUBEX parameter (marked as Grell-AS, blue); and New parameters (light green) for cluster number-10.

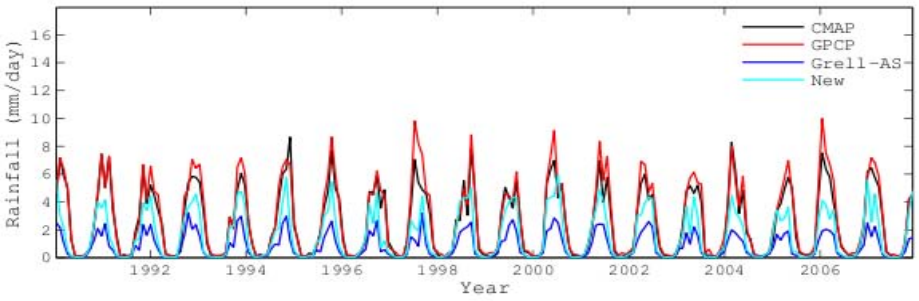

Figure 8.24: Rainfall time series: CMAP (black); GPCP (red); Old SUBEX parameter (marked as Grell-AS, blue); and New parameters (light green) for cluster number-11.

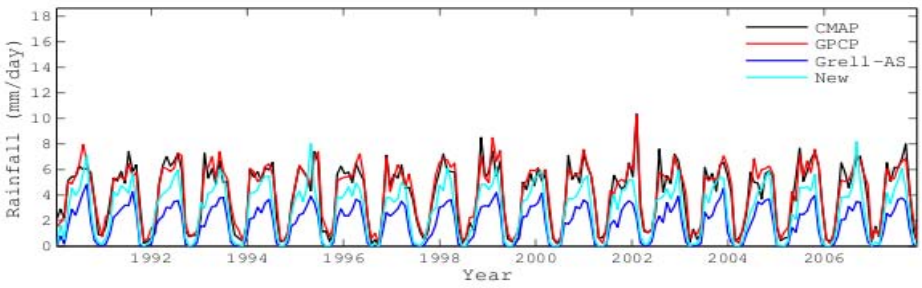

Figure 8.25: Rainfall time series: CMAP (black); GPCP (red); Old SUBEX parameter (marked as Grell-AS, blue); and New parameters (light green) for cluster number-12.

Chapter 9

CONCLUSION

The nonconvective precipitation, which is parameterized through subgrid explicit moisture scheme (SUBEX) in RegCM4 and its predecessors, is improved through optimal set of parameters for the horn of Africa region. The optimal set of SUBEX parameters are selected such that there is a large and significant correlation of simulated precipitation with observed precipitation of CMAP and GPCP; there is small RMSE and Bias in RegCM4 precipitation compared to these data set. The RegCM4 precipitation is obtained from a simulation which encompasses a domain covering 39.9 degree west to 80.44 degree east and 24.6 degree south to 25.1 degree north on 60 km horizontal resolution and 18 vertical levels. The asymmetry in north-south direction is due to the requirement that the map scale factor should be close to one. ERA-INTERIM data set of ECMWF is used for initial and lateral boundry conditions. SST from weekly-IO is used to drive the model.

The majority of the sensitivity (about 84 model runs) are performed for the JJAS months of normal year 2000. This is important to avoid forced bias of the simulated climate variables towards El Niño or La Niña years, both of which are extremes. After optimal set of parameters are selected we run the model for two long years: one in the defualt setting and the other in the new parameters setting.

We have found optimal set of parameters which has significantly reduced the existing descrepancy between observation and simulated rainfall by RegCM4. This is evaluated

using correlation, RMSE and bias with respect to the two data set. The comparison of the two long years runs have shown significant difference between the simulations. To assess wether the new parameters have altered the simulated precipitation in the direction which agrees with observation, we have compared both simulations with CMAP and GPCP. The result of the comparison has shown that there are significant improvements for some of the clusters located in north-western part of horn of Africa which includes western Ethiopia highlands and low lands as well as part of Sudan. There are also some clusters with significant improvement on south-western of the region. However, low lying regions in south-easter which includes south-eastern part of Ethiopia, Somalia, part of Kenya and adjoining Indean Ocean have shown little or no change in capturing the observed precipitation pattern and inter annual variations. This is probably an indication that further improvements are needed in particular with respect to rain drop evaporation rate. In summary, we have found better set of parameters that can replace the old parameters for further climate studies over the western and south-western and north-western part of the horn of Africa.

Bibliography

[1] Arakawa, A., and W. H. Schubert, Interaction of a cumulus cloud ensemble with the large-scale environment, part I, J. Atmos. Sci., 31, 674 701, 1974.

[2] Ashock, Karumuri, Z. Guan, and T. Yamagata, 2003: A look at the relationship between ENSO and the Indian Ocean Dipole. J. Meteor. Soc. Japan, 81, No 1, 41-56.

[3] Behera, S. K., J. Luo, S. Masson, P. Delecluse, S. Gualdi, A. Navarra, and T. Yamagata, 2005: Paramount impact of the Indian Ocean Dipole on the East Africa short rains: A CGCM study. J. Climate, 18 (21), 4514-4530.

[4] Beltrando G and P. Camberlin, 1993: Interannual variability of rainfall in the eastern Horn of Africa and indicators of atmospheric circulation. Inter. J. Climatol., 13: 533546.

[5] Beltrando, G., 1990: Space-time variability in April and October-November over East Africa during the period 1932-1983. J. Climatol., 10, 691-702.

[6] Black E., J. Slingo, and K. Sperber, 2003: An observational study of the relation ship between excessively strong short rains in coastal East Africa and Indian Ocean SST. Mon. Wea. Rev. 131, 7494.

[7] Dickinson, R. E., A. Henderson-Sellers, and P. J. Kennedy, 1993: Biosphere-atmosphere transfer scheme (bats) version 1e as coupled to the ncar community climate model, Tech. rep., National Center for Atmospheric Research.

[8] Farmer, G. 1988: Seasonal forecasting of the Kenya coast short rains, 19011984. J. Climatol., 8, 489497.

[9] Hastenrath S., Nicklis A., and Greischar L., 1993: Atmospherichydrospheric mecha nisms of climate anomalies in the western equatorial Indian Ocean. J. Geophys. Res.: Oceans, 98, 2021920235.

[10] Holtslag, A. A. M., E. I. F. de Bruijn, and H.-L. Pan, 1990: A high resolution air mass transformation model for short-range weather forecasting, Mon. Wea. Rev., 118, 15611575.

[11] Hsie, E. Y., R. A. Anthes, and D. Keyser, 1984: Numerical simulation of frontogenisis in a moist atmosphere, J. Atmos. Sci., 41, 25812594.

[12] Hutchinson P., 1992: The Southern Oscillation and the prediction of Der season rainfall in Somalia. J. Clim., 5, 525531.

[13] Murphree, T., 2005: MR3610 Course Module 5: Introduction to Climate Science. Department of Meteorology, Naval Postgraduate School, Monterey, California, 45 pp.

[14] Nicholson and J. C. Selato, 2000: The influence of La Nina on African Rainfall. Int. J. Climatol., 20, 1761-1776.

[15] Nicholson , and J. Kim, 1997: The relationship of the El Nino-Southern Oscillation to African rainfall. Int. J. Climatol., 17, 117-135.

[16] Nicholson, S. E., 1997: An analysis of the ENSO signal in the tropical Atlantic and western Indian Oceans. Int. J. Climatol., 17, 345-375.

[17] Ogallo, L. J., 1988: Relationship between seasonal rainfall in East Africa and the Southern Oscillation, J. Climatol., 8, 31-43.

[18] Philander, G. S., 1990: El Nino, La Nina, and the Southern Oscillation. Academic Press, San Diego.

[19] Ramage, C., 1971: Monsoon Meteorology. International Geophysics Series, Vol. 15, Academic Press, 296 pp.

[20] Ropelewski, F., and M. S. Halpert, 1987: Global and regional scale precipitation patterns associated with the El Nio/Southern Oscillation. Mon. Wea. Rev., 115, 1602-1626.

[21] Saji, N. H., B. N. Goswami, P. N. Vinayachandran, and T. Yamagata, 2002: A dipole mode in the tropical Indian Ocean. Nature, 401, 360-363.

[22] Slingo, J., 2003: Monsoon overview, Encyclopedia of Atmospheric Sciences. pp. 1365 1370. Elsevier Science Ltd..

[23] Vojtesak, Michael M., K. Martin, and G. Myles, 1990. SWANEA (Southwest Asia-Northeast Africa): A Climatological study. Volume 1The Horn of Africa. SAFETAC TN-90/004, USAF Environmental Technical Applications Center, Scott AFB, Illinois, 249 pp.

Declaration

This thesis is my original work, has not been presented for a degree in any other University and that all the sources of material used for the thesis have been dully acknowledged.

Name: ABEBE KEBEDE H/GEBRIEL

Signature:————————

Place and time of submission: Addis Ababa University, June 2011
This thesis has been submitted for examination with my approval as University advisor.

Name: DR. GIZAW MENGISTU

Signature:————————